Thesis for The Degree of Licentiate of Engineering

Consideration of the non-linear behaviour of joints for efficient design of complex timber structures

Dorotea Caprio

Department of Architecture and Civil Engineering
Gothenburg, Sweden, 2023

Consideration of the non-linear behaviour of joints for efficient design of complex timber structures

Dorotea Caprio

Technical Report No 2023:2
Lic /Architecture and Civil Engineering / Chalmers University of Technology

Department of Architecture and Civil Engineering
Division of Structural Engineering
Group of Lightweight structures
SE-412 96 Göteborg,
Sweden
Phone: +46(0)31 772 1000

Cover:
The picture shows the multi-level approach on which the present work is based: the single-fastener joint level, the multi-fastener joint level and the structure level.

Printed by Chalmers Digitaltryck,
Gothenburg, Sweden 2023.

“Education really is the job of a lifetime.
And it commences: now.“
This is water, David Foster Wallace

Consideration of the non-linear behaviour of joints for efficient design of complex timber structures

Dorotea Caprio

Department of Architecture and Civil Engineering

Abstract

The re-emergence of timber as a construction material, facilitated by the development of modern engineered wood products, has enabled the creation of modern and complex timber structures. A detailed description of the load-displacement curves of timber joints is required. However, current design rules based on a semi-probabilistic design concept, do not capture the interactions among the components (system effects). In this regard, a reliability approach is more appropriate for evaluating the system effects and safety of the entire system. However, the estimation of the reliability of complex structural systems can be demanding in terms of computational effort and accuracy.

In this thesis, the impact of the non-linear behaviour of joints has been assessed by performing a parametric study on a simple but representative structure (beam supported by rotational springs at the ends). The uncertainties arising from the load, material characteristics, and the mechanical behaviour of joints were considered in the analysis. Different methods to estimate the reliability of a structure, such as Crude Monte Carlo, Important sampling, and metamodel-based techniques, were compared in terms of computational time and precision. Results showed that Crude Monte Carlo was the most adequate compared to other methods since the probability of failure was estimated with good accuracy and relatively small computational time. It was found that the probability of failure of the structure is sensitive to the elastic stiffness and ductility of the joints and their variability. However, a simple elastic-perfectly plastic model for joints is not representative of all the load-displacement curves of the joints. For this reason, regression models were applied to relevant load-displacement curves from the literature and their suitability for approximating diverse load-displacement curves was evaluated. The Richard-Abbott model was found to be the most appropriate for approximating the load-displacement shapes of joints and the associated variability.

This work provides the basis for a reliability-based approach for the analysis of structural systems, where the impact of joints on the performance of a structure is assessed and quantified. This will enable a more rational design of modern timber structures.

Keywords

connections, joints, elastic stiffness, ductility, reliability-based, regression models

List of Publications

Appended publications

This thesis is based on the following publications:

[**Paper I**] **D. Caprio**, R. Jockwer, M. al-Emrani, *Reliability of statically indeterminate structures: modelling approaches and sensitivity study Current Perspectives and New Directions in Mechanics, Modelling and Design of Structural Systems (2022), RC Press, pp. 1649–1655, isbn: 9781003348443. doi: 10.1201/9781003348443-270.*

[**Paper II**] **D. Caprio**, R. Jockwer, *Regression models for the description of the behaviour of modern timber joints (2023) Submitted for publication.*

AUTHOR'S CONTRIBUTION TO JOINTLY WRITTEN PAPERS

The appended papers were written in collaboration with co-authors. The contribution of the author of this licentiate thesis to the appended papers is described in the following:

In **Paper I**, the author was responsable for the majority of planning and writing of the paper. The author developed the analytical model, performed the statistical analysis and was responsible for the results, discussion and conclusions;

In **Paper II**, the author was responsable for the majority of planning and writing of the paper. The author performed the literature review, the analysis and was responsable for the results, discussion and conclusions.

Other publications

In addition to the appended papers, the author has also contributed to the following published or under review papers:

[**a**] R. Jockwer, **D. Caprio**, A. Jorissen, *Evaluation of parameters influencing the load-deformation behaviour of connections with laterally loaded dowel-type fasteners*
Wood Material Science Engineering, vol. 17, pp. 1–14, Jul. 2021. doi: 10.1080/17480272.2021.1955297.

[**b**] R. Jockwer, **D. Caprio**, *Reliability of complex timber structures: impact of connection non-linearity and overstrength*
Submitted to the 14th International Conference on Applications of Statistics and Probability in Civil Engineering, ICASP14 Dublin, Ireland, July 9-13, 2023.

Acknowledgment

The work presented in this thesis was conducted at the Division of Structural Engineering, at Chalmers University of Technology, between October 2020 and March 2023. The research project was funded by Svensk Trä, the Swedish association of the timber industries, and TMF, the Swedish Federation of Wood and Furniture Industry, to which the author expresses her gratitude.
I am grateful to my supervisors, Robert Jockwer and Mohammad al-Emrani, for their trust in me and for the opportunity to spend time studying this fascinating subject. In particular, I want to thank Robert for his valuable feedback, for letting me learn by making mistakes without feeling judged, and for the valuable discussions. To Mohammad for the knowledge and wisdom, for leaving his office door open for anything I wished to discuss. It is impossible to not mention my examiner Karin Lundgren, whose advice and feedback further improved my work.
I would also like to express my gratitude to all the members of the Lightweight structure group. Leaving my country and family was not easy, but you somehow became a new family. I am looking forward to future weekly badminton matches. Special thanks to Fatima, one of the kindest person I know and to Vera, the new member of the office whose company I really appreciate. Finally, I cannot forget to thank all my colleagues and peers with whom I shared my lunch breaks and fika. You made office life far less boring.
I would also like to thank my family and friends from Italy. Leaving you behind was not easy, but you always supported me. A special to Cristina, my concert buddy and lifelong friend. I hope to see you soon somewhere in Europe.
Finally, I want to thank my boyfriend Daniele. Without you, the mathematical formalism of this thesis would not have been so accurate. You are the reason why I am doing what I love and the reason why I believe I could do it.

Contents

Abstract iii

List of Publications v

Acknowledgement vii

I Summary 1

1 Introduction 3
- 1.1 Background . . . 3
- 1.2 Scope and objectives . . . 5
- 1.3 Research methodology . . . 6
- 1.4 Limitations . . . 9
- 1.5 Outline . . . 9

2 State of the art 11
- 2.1 Modern and complex timber structures . . . 11
  - 2.1.1 Large span structures . . . 11
  - 2.1.2 Tall timber buildings . . . 18
- 2.2 Basis of design . . . 20
  - 2.2.1 Types of structural analysis . . . 20
  - 2.2.2 Structural engineering decision making . . . 21
  - 2.2.3 Methods for the reliability estimation . . . 23
- 2.3 Behaviour and design of joints in timber structures . . . 27
  - 2.3.1 General . . . 27
  - 2.3.2 Analytical models . . . 28
  - 2.3.3 Design of timber joints according to standards . . . 30
  - 2.3.4 Load-displacement shapes of timber joints . . . 36

3 Reliability estimation of the structure 39
- 3.1 Case study . . . 39
- 3.2 Implementation . . . 40
- 3.3 Methodology . . . 40

4 Results and discussion **43**
4.1 Parametric study 43
4.2 Load-displacement curves of joints 44
4.2.1 Model fit 46
4.2.2 Stability of the model 48

5 Conclusions and future work **51**
5.1 Conclusions 51
5.2 Future work 52

Bibliography **57**

Part I

Summary

Chapter 1

Introduction

1.1 Background

The use of wood as a building material started more than 10 millennia ago. Examples of ancient buildings still standing today are the 32.5 meters high Horyu-ji Temple in Nara, Japan, one of the oldest wooden churches in the world, the Greensted Church in the UK from 1053, or a currently inhabited farmhouse from the 11th century on the Faroe Islands [1]. Wood was a popular material until the middle of the 19th Century, when in Sweden and many other countries the use of wooden buildings was limited after several fires destroyed a large number of buildings. Consequently, the use of wood was restricted by building regulations. Wood was considered an old and "unsafe" technology. With the industrial revolution, concrete and steel became the principal construction materials, used in large and important projects such as the Eiffel Tower and the skyscrapers in Northern America, whereas timber became a material for smaller structures, such as residential light-frame housing [2].

(a) Horyu-ji Temple - Nara, Japan (b) Church of St.Andrew - England

Figure 1.1: Examples of ancient wood buildings

The need for more sustainable structures coupled with the development of engineered wood products, such as glulam (GLT), cross-laminated timber (CLT), and laminated veneer lumber (LVL), have created the right conditions

for the re-emergence of timber as an essential construction material [2]. As a result, there is growing interest in building large-span timber structures, tall buildings, and statically indeterminate structures [3].

Traditionally, concrete, steel, and timber buildings were constructed following experience and empirical rules rather than scientific theory. The design code for timber reflects the development and modernization of industrial sector to a lesser extent compared to those of steel and concrete [4].

This is also reflected in how the design of joints[1] is handled. Joints are the most sensitive parts of a structure because they govern the failure mode, the reliability, the robustness, the costs and the dynamic behaviour of the structure [6]. Their behaviour is often described in terms of elastic stiffness, load-carrying capacity and displacement capacity or ductility. Currently, the commonly employed approach to design timber structures is based on element-by-element verification. According to this concept, the load-carrying capacity of timber members and joints is checked against the effects of the loads [7]. According to Eurocode 5 (EC5, EN 1995-1-1 [7]), the load-carrying capacity of joints with laterally-loaded dowel-type fasteners can be calculated according to the well-known European Yield Model (EYM), while the stiffness at the serviceability limit state (SLS) is an empirically-based equation. Regarding other types of joints, such as joints with axially loaded glued-in rods (GiR), different approaches to calculate the load-carrying capacity can be found in literature [8], [9]. An equation depending on the bonded length and withdrawal strength has been proposed in the draft of the next generation of EC5 (prEN 1995-1-1) [10], while the corresponding equation of axial stiffness in SLS is taken from joints with self-tapping screws (STS). To consider the non-linear behaviour of joints at the ultimate limit state (ULS), the stiffness at SLS is reduced to two-thirds, based on models of nailed joints made of Australian hardwood [11]. Indications on how to design ductile joints are lacking in design standards. In the literature multiple definitions of ductility exist, which makes it difficult to compare different studies [12], [13].

These simplifications of the standards do not reflect the range of diverse and high-performance joints, that present non-linear load-displacement behaviour. In addition, the structures are designed and verified following a semi-probabilistic concept that does not capture system effects, i.e. the reliability of the entire structure might differ from the reliabilities of each individual component of the structures when this is considered separately. The entire complex timber structure needs to be analyzed as a system of interconnected elements, considering the interaction of all members and joints and accounting for the non-linear load-displacement behaviour of joints and the associated variability. These are important prerequisites to design reliable structures [14], [15]. Thus, a reliability-based approach looks more appropriate to estimate the probability of failure of the structures [14] and analytical models can be used to approximate the joints behaviour.

[1]The terms 'joint' and 'connection' are often used as synonyms in the literature. In [5] the joint is defined as the union of two or more joints and the joint is defined as an ensemble of fasteners with two or more members. In this paper, for the sake of the clarity of the reader, the term "joint" is used to indicate a connection.

In this study, different methods to estimate the reliability of the structure will be tested and compared in terms of efficiency and computational time, then a parametric study varying stiffness and ductility of joints with consideration of their variability was conducted on a simple statically indeterminate system, i.e. a simple beam with rotational springs at its supports. The most influential characteristics of the joint on the reliability of the structure were identified. In the parametric study, the load-displacement behaviour of joints was considered elastic-plastic. This simplified approximation of joints was compared with load-displacement curves of different joints retrieved from the literature. The current design rules are applied and the need for a more precise description of timber joints is underlined. For this scope, different analytical models for approximating the highly non-linear behaviour of joints were reviewed and assessed. The Richard-Abbott model was selected since it could approximate all the analyzed load-displacement curves and represent the variability associated with the experimental data. The analytical model will serve as a basis for updating the reliability-based model considering the semi-rigidity of joints and the uncertainties connected to the estimation of their load-carrying behaviour.

1.2 Scope and objectives

This thesis aims to assess and quantify the influence of joints non-linear behaviour and related uncertainties on the failure probability of a complex structural system. Based on the results of the analysis, design recommendations on the design of timber joints will be given. Within this aim, the following objectives were identified:

(i) to compare existing methods for estimating the probability of failure of complex timber structures;

(ii) to identify relevant characteristics of the load-displacement of joints affecting the reliability of a representative complex structure;

(iii) to identify the most suitable analytical model to represent the non-linear behaviour of joints and the related variability.

Although not answered in this thesis, additional objectives were identified to meet the overall aim of the project. The following objectives were taken into account for the work presented in this thesis, though their results will be addressed in future work:

(i) to develop a model for the description of the non-linear behaviour of the single-fastener joint and to quantify the variability of the model parameters by means of experiments on the single-fastener joint;

(ii) to develop a model for the description of the non-linear behaviour of multi-fastener joints, using the model for the single fastener joint as input;

(iii) to perform a structural analysis of the entire structure considering the non-linear behaviour of joints and the related uncertainties developed in the previously described objectives.

1.3 Research methodology

In order to meet the aim of the project, system effects within a structure have to be considered. In fact, a structure is a system made of multiple and interconnected components whose joints should be taken into account in order to assess the actual reliability of the structure. The latter is affected by the non-linear behaviour of the multi-fasteners joints, which is a consequence of the non-linear behaviour of the single fastener.

This project is carried out by using a multi-level approach according to which the structure is analyzed at three different scales: the single-fastener joint, the multi-fastener joint and the whole structure. This multi-level approach is illustrated in Figure 1.2.

The model describing the behaviour of a single fastener can be used as input for the model representing the behaviour of the multi-fastener joint. The resulting load-displacement curve can subsequently be used as input for the analysis of the entire structure in order to assess the influence of joints behaviour on the reliability of the structure. In this study, it has been decided to start from the analysis of the structure using a simplified but non-linear model of joint behaviour, with reasonable assumptions of the uncertainties related to stiffness and ductility. Reliability methods are compared in this step in terms of efficiency and computational time and the most suitable one was chosen to conduct this analysis was identified. The most impacting characteristics of the joint on the performance and safety against collapse of the structures are highlighted.

In light of results coming from the analysis of the entire structure, the appropriate joints can be studied, focusing only on the aspects that have been identified as relevant. Then, the single fastener behaviour can be studied and used as input for the multi-fasteners model. The model of the entire structure can then be updated with a more precise description of the load-displacement curve of joints and related uncertainties. The work performed in this thesis and the link to future work is described in Figure 1.3. Paper I concerns the structure level, with simplifications on the load-displacement curve of joints and related variability/uncertainties. Paper II identifies a suitable analytical model that will be used in future work for the development of the single-fastener joint model.

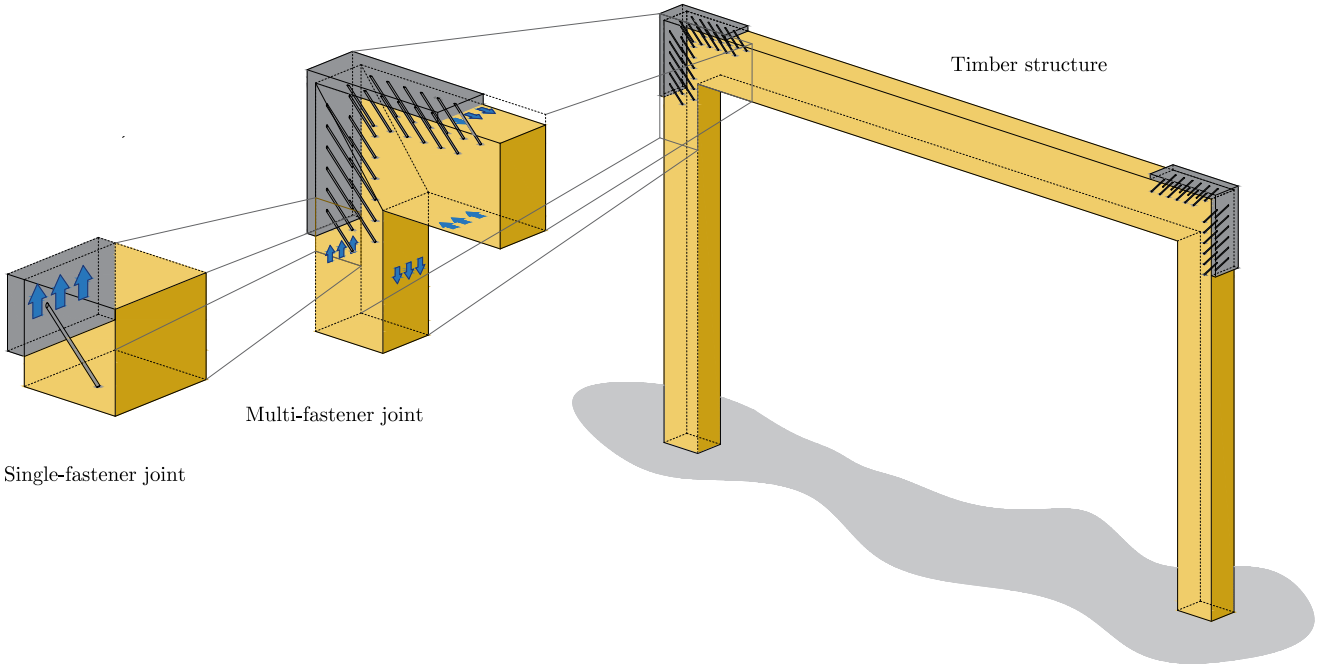

Figure 1.2: Multi-level approach. Three levels are considered: the single fastener joint, the multi-fastener joint, the structure. Figure inspired by the drawing `https://lnu.se/en/research/research-groups/connections-in-timber-structures/`

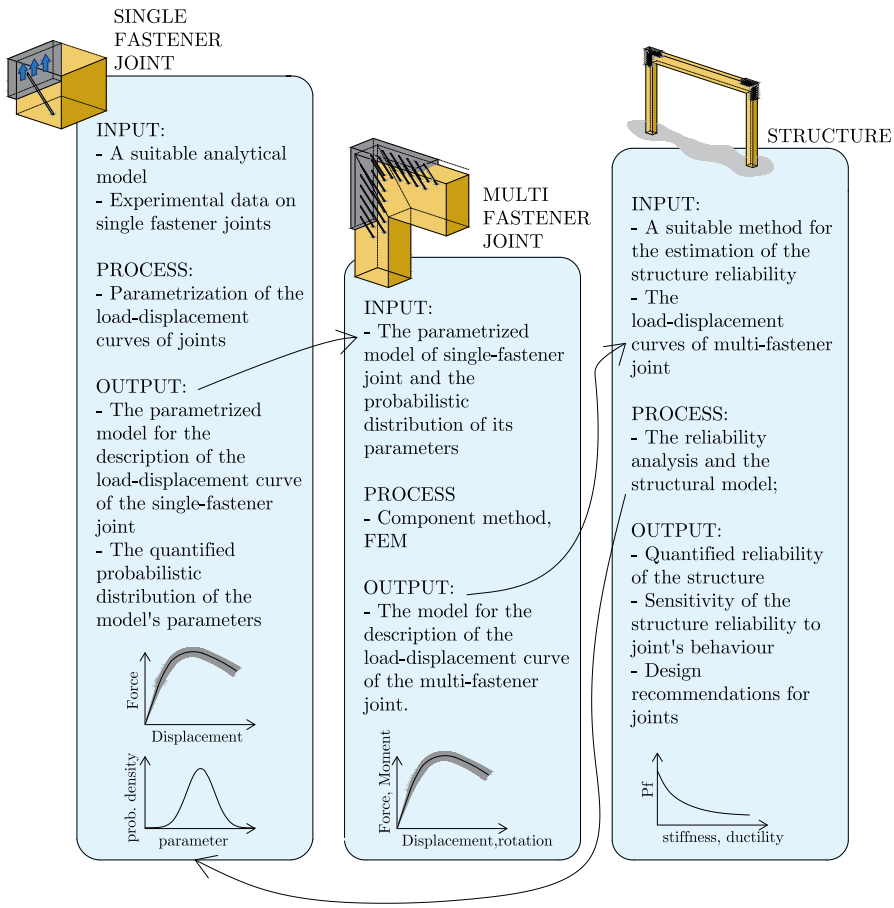

Figure 1.3: Overview of the work presented in this thesis and its link to future work.

1.4 Limitations

The limitations of the work are herein summarized:

1. The reliability of a simple but representative case of a statically indeterminate structure was estimated. However, only two joints are present in the structure. This example might not capture the effect of redundancy on the reliability against the collapse of larger structural systems;

2. The probability distributions assigned to the rotational stiffness and ductility of the joints are based on assumptions. None or little information on which distribution to consider can be found in literature or design codes;

3. The available load-displacement curves of joints from the state-of-art are the results of experimental tests conducted following current testing standard EN 26891 [16]. Some of the experiments have been stopped at a displacement of 15 mm, so before a considerable load-drop or maximum load was reached, therefore they do not represent the total load-displacement curve shape;

1.5 Outline

This thesis consists of an introductory part and two appended papers.

Chapter 1 provides the background of the work and it explains the aim, the method, and the limitations of the study;

Chapter 2 introduces the theoretical framework of the work by reviewing the state-of-art of modern timber structures and joints, the current design approaches of timber joints and timber structures, and methods to estimate the reliability of a structure;

Chapter 3 illustrates the results of the comparison among different methods to estimate the reliability of a structure;

Chapter 4 shows the main findings of the parametric and sensitivity analysis on the case study after a suitable method to estimate the reliability was selected. In this chapter, the suitability of the analytical models to represent the load-displacement curves of joints is tested on selected load-displacement curves from the literature.

Chapter 5 presents the main results of the present work and gives suggestions for future work.

Chapter 2

State of the art

2.1 Modern and complex timber structures

2.1.1 Large span structures

Large-span structures and tall timber buildings are examples of the renaissance of timber as a building material. Among one-span structural systems for large-span structures, we find simply supported beams or portal frames, trusses, arches, and suspension systems. The order in which they are listed represents the increasing order of structural efficiency [17], [18] (Figure 2.1).

The effects of loads on a straight beam element depend by the rotational stiffness of the joints. If the joints have zero stiffness, the moment at the centre of the beam will be maximum, while if the joints are semi-rigid, the moment at the midspan will be reduced, resulting in a smaller required cross-section of the beam (Figure 2.2).

A portal frame is a type of large-span structure system with moment-resisting joints (MRJs). MRJs can reduce the need for bracing with diagonal members or walls and therefore allow for a more open and flexible architecture, or in the case of beam-to-beam joints, to allow larger spans [19]. In a portal frame, the joints are considered rigid or semi-rigid. This makes the structure statically indeterminate. Examples of employed joints are joints with dowel-type fasteners (DTF), considered semi-rigid, and glued finger-joints, considered fully rigid [14], [20] (Figure 2.3). In the case of joints with dowels, different load orientations can be present in multi-dowel joints, which consequently leads to an unequal distribution of the load to the individual dowels. Finger-joints are not ductile and are challenging to manufacture onsite. The frame corner can also be realized using glued-in rods alone or together with steel profiles [21].

In a structure in bending, like a simple straight beam, the stress is not uniform in the section: it varies linearly from a maximum compression stress to a maximum tensile stress. Trusses are more structurally efficient because the loads are transferred through compression and tension forces inside the members [17]. Usually, the design of compression members is governed by buckling and the design members in tension by the tension resistance of the

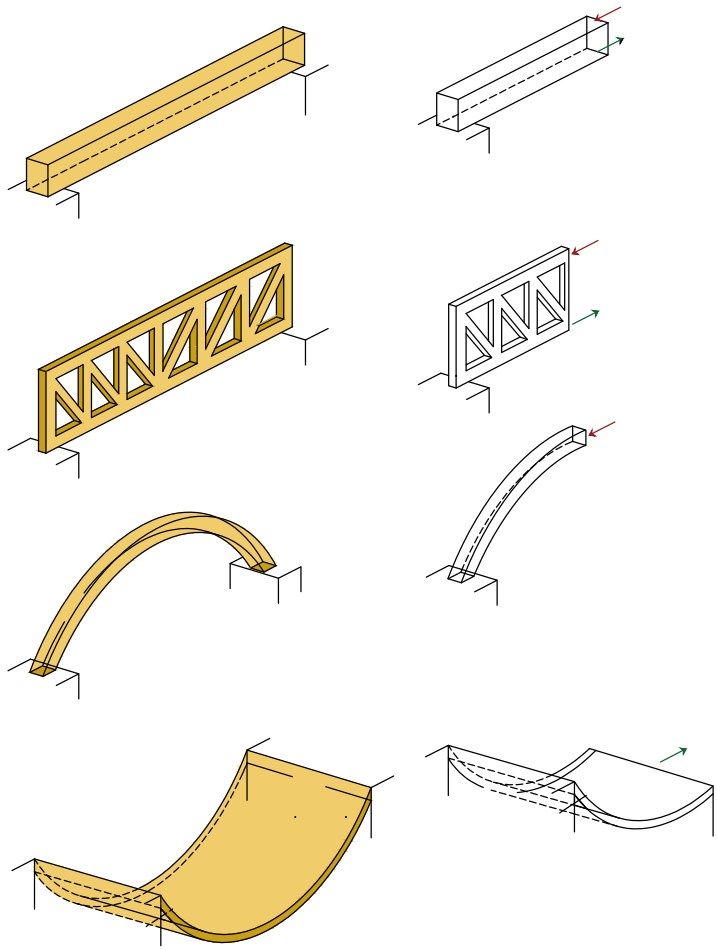

Figure 2.1: Different structural systems: a beam, a truss, an arch, and a tension structure

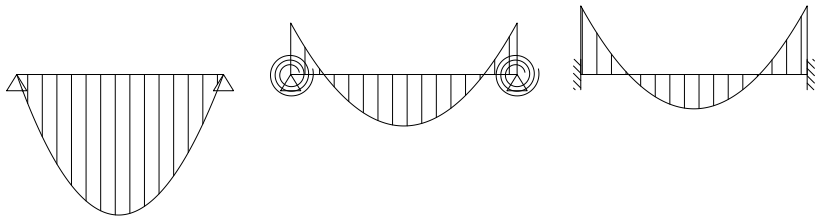

Figure 2.2: From left to right: simply supported beam, beam with the semi-rigid joints and beam with the clamped joints

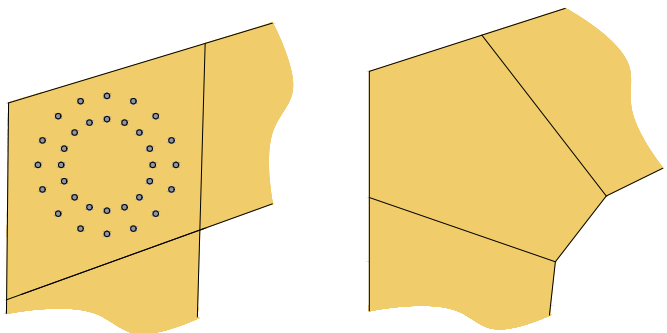

Figure 2.3: Examples of MRJs in a portal frame: left a joint with laterally-loaded dowels, right: a finger-joint

weakest points, i.e. the joints [17]. Trusses are composed of one of the more triangular units made of rigid members and connected by joints. The joints are usually considered pinned, even if they can be loaded with moments due to eccentricities [22]. Two examples of possible joints are illustrated in Figure 2.4. The first one is composed of laterally-loaded dowels and slotted-in steel plates, while the second is composed of laterally-loaded bolts and outer steel plates.

An example of a timber truss is the Messe Frankfurt Hall manufactured by WIEHAG [23] (Figures 2.5(a) and 2.5(b)). The roof is made of 12 timber trusses realized with steel tie diagonals in the interior of the hall and timber frames at the tapered edge of the roof. The span is 78 m. The joints between the tension chord, the vertical members, and the diagonals are realized with inclined STS, while the joint of the cantilever truss was realized using slotted-in steel plates and dowels. These joints were also reinforced using screws.

In arches, the influence of the moment can be partially avoided since the shape can be chosen to follow the thrust line of the dominant load combination [17]. Vertical loads are mostly translated into compression forces in the arch, but horizontal loading will produce bending moments. These can be reduced by

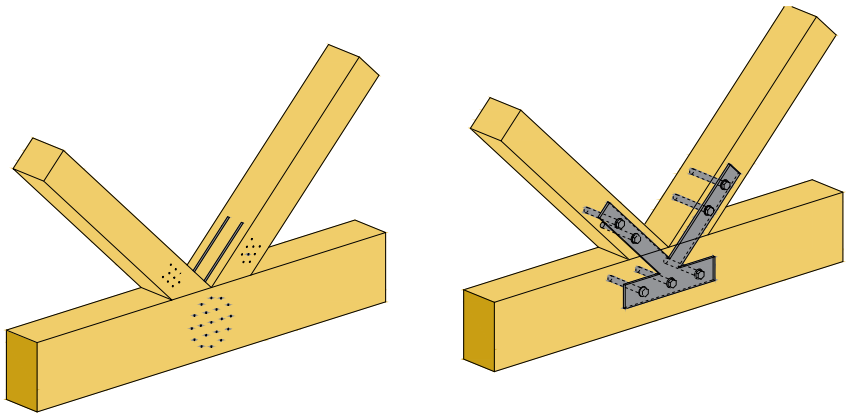

Figure 2.4: Example of joints in truss structures. Left, joints with slotted-in metal plates and laterally-loaded dowels; right: joints realized with external steel plate and bolts

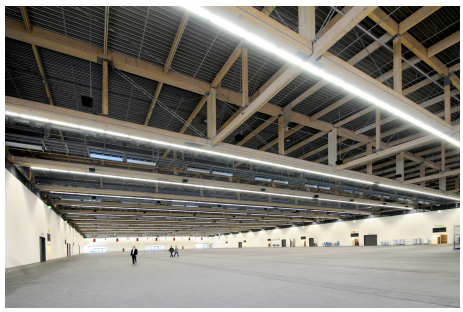

(a) Messe Frankufurt Hall (inside), Germany - © Max Bögl/WIEHAG

(b) Messe Frankufurt Hall (outside), Germany - © Messe Frankfurt GmbH, Arch. Hascher Jehle/WIEHAG

Figure 2.5: Messe Frankufurt Hall

choosing appropriate arch shapes [17], [18]. Arches can be statically determinate

(three-hinged arches) and statically indeterminate (two hinged arches) (Figure 2.6) [17], [18]. Three-hinged arches are used for spans up to 60-70 m, while larger spans require the arch to be transported in more parts, that are later connected on site [17]. An example of an interior joint that restores the continuity of the arch is the one realized for the Nanyang Technological University Sports Hall, Singapore [24] (Figures 2.8(a) and 2.8(b)). The joint is realized by steel plates and inclined STS that resist tensile and compression forces from the moment, while symmetric central plates on each side provide strength against shear forces (Figure 2.7) [24].

Figure 2.6: Structural systems for arches: three hinged arch, three hinged arch with interior joints, two-hinged arch and interior joints

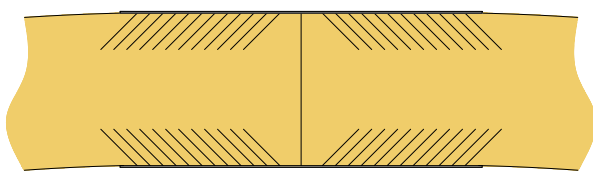

Figure 2.7: Illustration of the moment resisting joints made of inclined self-tapping screws and steel plates for the arch of the University Sport Hall (Singapore)

A timber roof can be realized using a suspended structure. Suspended structures are highly efficient because they take loads in tension. This means that their design is not governed by buckling failure, as in arches [17], [18].

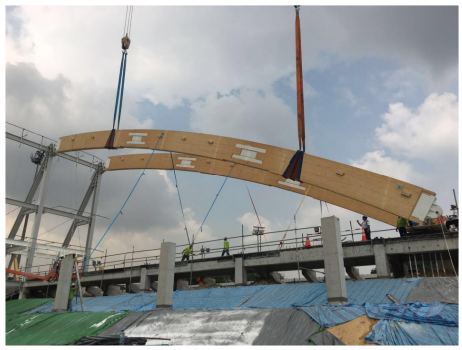

(a) Arch with moment resisting joints during construction © Ermanno Acler [24]

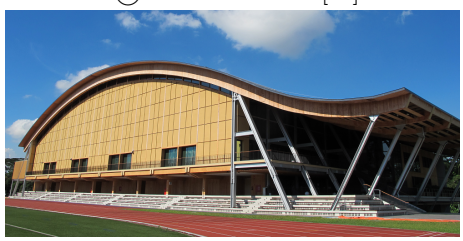

(b) Outside view of the roof arch © Ermanno Acler [24]

Figure 2.8: University Sport Hall, Singapore

Special structures

Computational technology makes it possible to build complex and innovative timber structures. Domes and gridshells are unique timber structures. In these structures, the effects of the loads are translated into compression and tension forces in the members. A popular type of dome is a geodesic dome composed of triangles that possess local rigidity and that can distribute the forces throughout the geodesic sphere. Therefore, this type of structure does not require additional bracing. In the design, the joints of reticular domes are often considered pinned or rigid due to the lack of information about their actual mechanical behaviour.

Despite these simplifications about their mechanical behaviour, the joints play an essential role in the performance and failure of these types of structures [25]. Members in compression are sensitive to buckling failure and the boundary conditions of a member (whether a joint is considered fixed or hinged) might change the ultimate load of the structure. An example of a reticular dome is situated in Brindisi, Italy (Figure 2.9). In this dome, the joints were realized with steel plate and inclined STS to resist the high moment and shear forces that arise in the construction phase [17].

Free-form domes can be grid shells. Traditionally, the gridshell shape is

(a) Dome structure in Italy © Oliver Jaist Fotografie

(b) Dome structure (inside) © Oliver Jaist Fotografie

Figure 2.9: Dome structure in Brindisi, Italy

selected in order to maximize the use of the structural form, reducing as much as possible bending moments and torsion [26]. Therefore, the grid shell is efficient because it transfers forces primarily through in-plane membrane forces. However, like for domes, simplifications are often made on the rotational stiffness of joints. Assuming that the joints are rigid can be unconservative since the members are prone to buckling and stability issues [26]. An example of a modern gridshell is the 310 m-long roof of Crossrail Place, Canary Wharf, London (Figure 2.10(a)). The beams are straight members and the curvature of the structure is created inside the joint. For this reason, the joint is characterized by high complexity (Figure 2.10(b)) [26].

(a) Crossrail station Canary Wharf, London © Foster + Partners/WIEHAG

(b) Detail of the joint, Crossrail station Canary Wharf, London © Nigel Young/WIEHAG

Figure 2.10: Crossrail Canalry Wharf, London

2.1.2 Tall timber buildings

Interest in building tall timber buildings is increasing in the construction industry, as seen by recently completed engineering projects of timber buildings. Tall timber buildings can be constructed using only timber or combined with steel or concrete. Tall buildings are typically built using CLT walls or GLT elements with an extensive trusswork bracing system.

An example of a truss typology is the tall building Treet, in Norway. With its 14 storeys one of the tallest timber buildings at its time of construction [27]. The Treet building has the truss structure on the facade similar to many bridges, that represent the main load-bearing structure. In addition, a core made of CLT elements is present at the centre of the building, which constitutes the vertical bearing for the stairs and elevators. The load bearing structure slightly supports the CLT elements. Still, the CLT structure has an insignificant contribution to the global stiffness of the overall building since the GLT trusses along the facade give the building the necessary global stiffness [27]. The joints are realized with slotted-in steel plates and dowels and they have been assumed pinned during the design.

Many examples of CLT-based tall timber buildings have been constructed all around the world [28]. For example, the residential complex Via Cenni, in Milan,

Stockholm's first residential CLT building, located in Sundbyberg, the Bridport House in London, which is part of a social housing project, or WoodCube in Hamburg [28]. Commonly employed joints in CLT-based structures are those realized with STS in floor-to-floor joints or in wall-to-wall joints. Moreover, to realize wall-foundation joints or wall-to-floor joints hold-on brackets and angle brackets are usually employed, using nails, bolts, or STS (Figure 2.11) [29]. Joints realized with hold-downs resist the uplift force, although they also possess a certain amount of lateral load-carrying capacity. Joints realized with angle brackets are primarily considered for shear forces, even if they also resist tension loads. The behaviour of a CLT wall is usually assumed rigid. Shear and bending deformations of the CLT panel are considered negligible compared to those of the joints. The main failure modes of a CLT wall are rocking, sliding, or a combination of the two. Therefore, the failure mode and the mechanical performance of a CLT wall under horizontal and vertical loading are greatly affected by the mechanical behaviour of joints [29], [30].

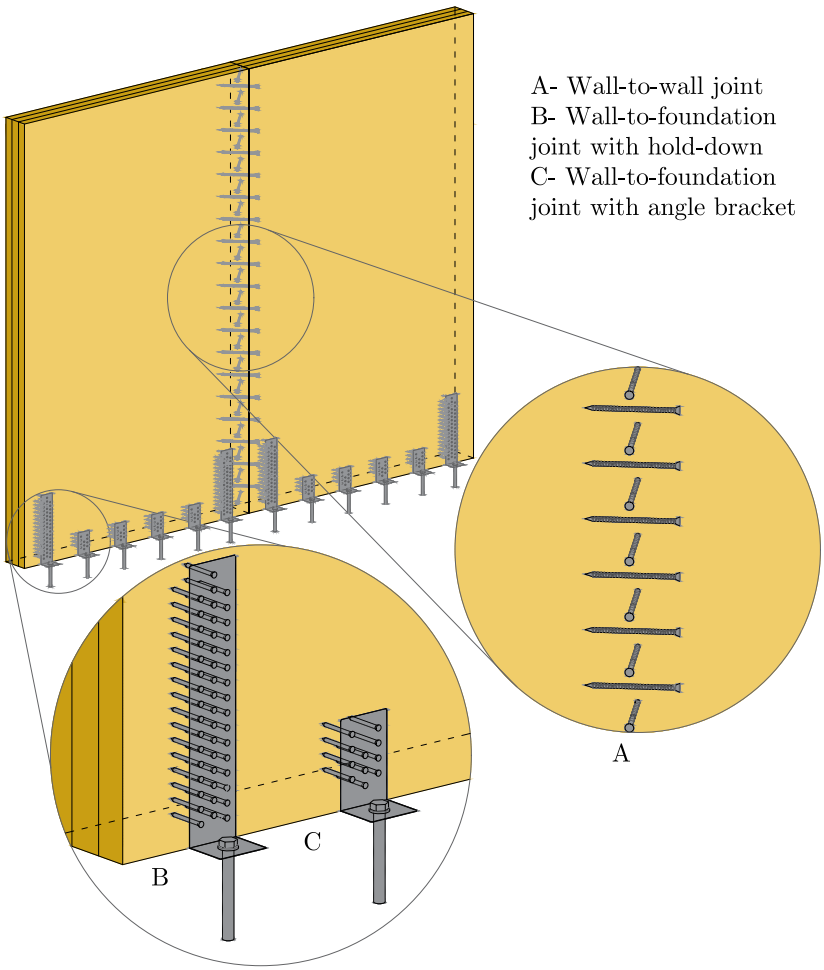

Figure 2.11: Typical joints in CLT-based structure

2.2 Basis of design

2.2.1 Types of structural analysis

Once the type of structure has been defined, it has to be ensured that it can resist the effects of the loads. This means that the following has to be satisfied:

$$S \leq R \tag{2.1}$$

Where S is the effect of the loads on the structure and R is the resistance of the structure. Three different types of structural analysis can be distinguished. They differ in the way the effects of the load and the resistance of the structural member are calculated.

In the elastic analysis, it is assumed that the material behaves in a linear-

elastic manner. The distribution of loads within the structure is determined by the elastic stiffness of the members and the resistance of the structure is reached when the material's yielding or proportional limit stress is reached at the most loaded point in the structure. Thus, the Equation 2.1 becomes:

$$\sigma_S \leq \sigma_y \tag{2.2}$$

Where σ_S is the stress provoked by the loads and σ_y is yielding stress or proportional limit stress of the material. In this type of analysis, if the material is ductile and there is potential for load re-distribution, the structure has great reserve of resistance.

According to elastic-plastic analysis, the loads are determined by elastic theory (the principle of superposition is valid) and the resistance by plastic theory, i.e. allowing the plastic resistance to be reached within a section. This type of analysis is typically applied to steel and concrete structures. Thus, Equation 2.1 becomes:

$$S_E \leq R_{pl} \tag{2.3}$$

Where S_E are the effects of the loads (computed according to elastic theory) and R_{pl} is the plastic resistance of the section.

In the plastic-plastic analysis, the effects on the structure are calculated according to the plastic theory. For example, in a statically indeterminate structure, such as a simply supported beam with fixed ends, a plastic mechanism can take place as long as a certain over-strength of the beam and rotational capacity of joints exist. Once the plastic moment is reached at the joints sections, a load distribution can allow the beam to be additionally loaded. In this case, the equation 2.1 is transformed into [12]:

$$\begin{aligned} q_E &\leq q_u \\ \phi_E &\leq \phi_u \end{aligned} \tag{2.4}$$

Where q_E is the applied load, q_u is the ultimate load that the structural system can sustain, ϕ_E is the rotation caused by loads and $\phi_{u,Rd}$ is the rotation capacity of joints. When applying the plastic-plastic analysis, the structure has reached its full capacity and has no further reserve of resistance.

In EC5 [7], it is specified that the global structural behaviour should be verified with elastic analysis. However, for structures able to re-distribute the loads due to joints of adequate ductility, "elastic-plastic methods might be used for the calculation of forces in the member". However, no further details are provided [31].

2.2.2 Structural engineering decision making

Structural design can be defined as the process of making a decision in the presence of uncertainties [32]. The uncertainties come amongst others from the resistance, loads, or joint characteristics. The uncertainties can be divided into two categories: aleatory and epistemic [4], [33]. Aleatory uncertainties are

related to uncertainties that arise from natural phenomena, while epistemic uncertainties are related to the approximation and the incompleteness of mathematical models that are used to describe a phenomenon. Decision making concerning the design and assessment of structures is addressed in ISO 2394 [34]. Here three different levels of approaches are identified: risk-informed decision making, reliability-based design and semi-probabilistic design [32] (see Table 2.1).

Table 2.1: Different levels of decision making according to ISO 2394 [34]

	Applied when:	Objective:
Risk-informed decision making	Exceptional design situations in regard to uncertainties and consequences	Minimize the risk according to the subject who makes the decision
Reliability-based design	Unusual design situations	Satisfy reliability requirements
Semi-probabilistic	Usual design situations in regard to consequences and uncertianties	Verify deterministic criteria

The risk-informed decision making is the most complete approach. With risk-informed decision making, different alternatives to the problem are analyzed in the presence of uncertainties and associated with consequences. The consequences can be direct or indirect [35]. The outcome of a risk analysis is expressed as the product of the probability P_E that an event takes place and the associated consequences of the events c_E [35]:

$$R_E = P_E \cdot c_E \tag{2.5}$$

The second level is represented by a reliability-based design concept. The outcome of this approach is the probability of failure of a system in the presence of uncertainties. Each failure mode is expressed with limit state function $g(\mathbf{X})$ (also called performance function). It is expressed as the difference between resistance (capacity), R and load (demand), S, which depend on the vector of random variables $\mathbf{X}$:

$$g(\mathbf{X}) = R(\mathbf{X}) - S(\mathbf{X}) \tag{2.6}$$

The probability of failure can be expressed as:

$$P_f = P(g(\mathbf{X}) \leq 0) = \int_{D_f} f_{\mathbf{X}}(\mathbf{x}) d\mathbf{x} \tag{2.7}$$

Where $f_{\mathbf{X}}()$ is the probability density function of the vector of random variables $\mathbf{X}$ and D_f is the failure domain. The probability of failure can also be expressed as a reliability index, defined as:

$$\beta = -\phi^{-1}(P_f) \tag{2.8}$$

Where ϕ is the standard normal cumulative distribution function.

Since there is no exact solution to Equation 2.7, probabilistic methods can be used. These methods can be grouped into approximation methods, simulation methods or adaptive surrogate modelling-based methods [14]. According to a

reliability method, the calculated probabilities of failure or the reliability index β have to be compared to certain acceptable limits or targets:

$$\beta = -\phi^{-1}(P_f) \geq \beta_t \tag{2.9}$$

The target reliabilities are decided on past experience, i.e. specified as the inherent reliability of traditionally accepted design solutions [36], or it is based on formal calibration using risk-informed methods [32]. The choice of target reliabilities depends on different parameters such as the importance and type of the structure, the possible failure consequences, etc. For example, according to the Joint Committee of Structural Safety (JCSS) [37], the probability of failure and the related β is associated with certain consequences and cost of repair for a reference period of one year (Table 2.2).

Table 2.2: Target reliability index (and associated target failure probabilities) related to a one year reference period and ultimate limit states [37]

Cost of safety measures	Minor consequences of failure	Moderate consequences of failure	Large consequences of failure
High	$\beta = 3.1 (\approx P_f = 10^{-3})$	$\beta = 3.3 (\approx P_f = 10^{-4})$	$\beta = 3.7 (\approx P_f = 10^{-4})$
Normal	$\beta = 3.7 (\approx P_f = 10^{-4})$	$\beta = 4.2 (\approx P_f = 10^{-5})$	$\beta = 4.4 (\approx P_f = 10^{-5})$
Low	$\beta = 4.2 (\approx P_f = 10^{-5})$	$\beta = 4.4 (\approx P_f = 10^{-5})$	$\beta = 4.7 (\approx P_f = 10^{-6})$

With this type of approach, system effects can be included in the analysis. However, consequences (robustness, sustainability, etc.) are not taken explicitly into account. Current design codes are based on the so-called load and resistance factor design (LRFD), which follows a semi-probabilistic approach. The verification of load-bearing structures is based on deterministic quantities: the design value of resistance has to be larger than the design value of load effects. For example, for a timber beam subjected to permanent and variable load, the design check translates in:

$$z \cdot \frac{R_k}{\gamma_M} - G_k \cdot \gamma_G - Q_k \cdot \gamma_Q = 0 \tag{2.10}$$

Where R_k is the characteristic resistance of the material, G_k is the characteristic value of permanent loads and Q_k is the characteristic value of variable loads. $\gamma_M, \gamma_G, \gamma_Q$, are the partial (safety) factors of resistance, permanent load and variable load respectively, and z is the design factor [38]. The partial safety factors are calibrated by performing a structural analysis following a reliability-based concept. However, the check is done on a component/failure mode level and the interaction of failure modes in a structure, i.e. system effects, are not considered.

2.2.3 Methods for the reliability estimation

The methods for estimating the reliability of a structure can be divided into approximation methods, simulation methods or adaptive surrogate-modeling base methods [14].

Approximation methods like first order reliability method (FORM) or second order reliability method (SORM) typically employ a first or second

order linearization of the limit state $g(\mathbf{X}) = 0$ close to most likely failure point (MLFP), found through the resolution of an optimization problem. High non-linearity of limit state equation can results in inaccuracies of these methods [39].

Instead, sampling techniques use a large number of samples (Crude Monte Carlo). The probability of failure in Monte Carlo (MCS) is estimated as the ratio of the number of realizations corresponding to failure to the total number of evaluations:

$$P_f \approx \hat{P}_f = \frac{1}{N_{MC}} \sum_{i=0}^{N_{MC}} 1_{D_f}(x^i) \tag{2.11}$$

The smaller the probability of failure, the larger the number of required samples is. To overcome this issue, importance sampling (IS) or Subset Simulation (Subset) can be used to reduce the number of samples, without compromising the accuracy. The population of samples is centered around the MLFP while in Subset the failure probability is considered as the product of larger conditional failure probabilities. In this way, the problem of rare-event estimation is changed into a sequence of problems of more frequent events [14], [40].

Another technique to reduce the number of samples is surrogate model-based approaches. The limit state equation in this case is replaced by a metamodel such as Polynomial chaos expansion (PCE) or Gaussian process modeling, also known as Kriging. These samples, however, are generally not optimal to estimate the failure probability. Thus, a more sophisticated methodology called active learning can be used [41]. The so-called experimental design $(\mathbf{X}^i, \mathcal{Y}^i) : \mathcal{Y}^i = g(\mathbf{X}^i) \in \mathbb{R}, \mathbf{X}^i \in \mathbb{X} \subset \mathbb{X}^M$, $i = 1, ..., m_0$ is initially generated. Typically m_0 is chosen in the order of tens of input samples. After initialization, the algorithm follows a four steps loop:

1. A surrogate model is built using experimental design;

2. The probability of failure is estimated using the current surrogate model and an appropriate method to estimate the reliability;

3. The convergence of the algorithm is checked, according to the chosen convergence criterion. If the convergence criterion is met, the algorithm stops;

4. If the convergence criterion is not met, an enrichment of the experimental design is carried out by selecting one pair of sample points $\mathbf{X}^{enr}, g(\mathbf{X}^{enr})$. The points are selected according to the learning function, which gives information about which points are most likely to increase the accuracy of the surrogate;

In this work, APCK-Subset was tested together with MCS, Subset, and IS.

Illustration example

In this section, an example of a parallel system composed of three limit state functions similar to the example presented in [42] is used to illustrate the effectiveness of the methods mentioned above for rare event estimation. The performance functions are defined as follows:

$g_1(x_1, x_2) = x_2 - \frac{1}{3}x_1^2 + sin(x_1) - 0,5$
$g_2(x_1, x_2) = x_2 - (\frac{x_1-2}{2})^3 + cos(3x_1) - 0,5$
$g_3(x_1, x_2) = (x_1 - 4)^3$

Table 2.3: Distribution parameters of random variables for the problem

Input variables	Distribution	Mean Value	CoV
x_1	Lognormal	1	0.2
x_2	Lognormal	1	0.2

Where x_1 and x_2 are independent standard log-normal distributed random variables.

The probability of failure of the parallel system is defined by the following:

$$P_f = Prob[g_1(\mathbf{X}) \leq 0 \cap g_2(\mathbf{X}) \leq 0 \cap g_3(\mathbf{X}) \leq 0] \tag{2.12}$$

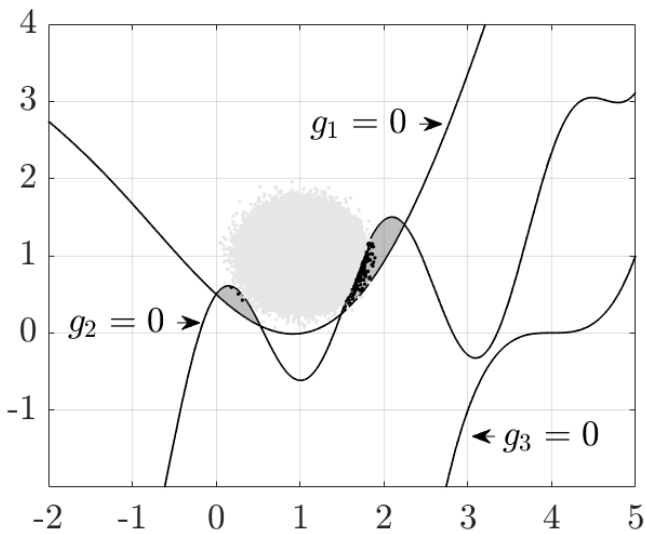

Figure 2.12: Three limit state equations. Samples belonging to MCS are represented with dots. Black points are the samples that fall into the failure domain

Subset reduces the number of samples needed, but it returns a higher value of the coefficient of variance (CoV). On the contrary, IS reduces even more the number of samples not at the expense of good accuracy. APCK-Subset

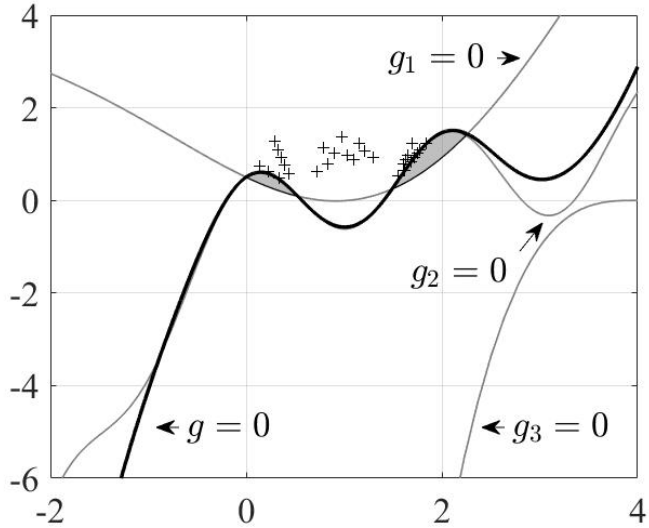

Figure 2.13: '+' points are the samples added by the active learning algorithm to reconstruct the limit state equation g

Table 2.4: Results for reliability problem. Different methods are compared in terms of computational time and accuracy

Method	Evaluations	P_f	CoV	Time
MCS	10^6	$2.00e^{-04}$	0.07	18.12 sec
Subset	3498	$2.01e^{-04}$	0.3	0.82 sec
IS	1067	$2.08e^{-04}$	0.06	0.82 sec
APCK-Subset	30	$2.05e^{-04}$	0.09	21.57 sec

is the method that needs fewer iterations since it is an iterative process, i.e. samples are added one by one. Thus, the computational time is higher than the computational time of other methods. However, in the presence of a finite element model, the necessity to reduce the simulation time may be a priority. In this case, this method is a good alternative to reduce computational time. Figure 2.13 compares the true model and its surrogate. The active learning algorithm accurately reconstructs the performance equations next to the failure domain. Therefore, it is unnecessary to have a precise fit of the surrogates to the true performance equations far from the system failure domain.

2.3 Behaviour and design of joints in timber structures

2.3.1 General

In general, the shape of the load-displacement curve differs for the different types of joints, however general characteristics can be identified. In particular, three regions can be characterized: "zero stiffness region" at low load levels, an elastic region, characterized by linear or quasi-linear relation between loads, and a plastic region at larger displacements. Brittle joints typically have load-displacement curves with little or no ductile region, while ductile joints have extended plastic regions. The stiffness at serviceability limit state K_{SLS} is used to describe the elastic region. K_{SLS} can be determined from the load-displacement curve, as the ratio of load divided by the corresponding displacement. Typically, it is evaluated as secant stiffness at a load level equal to $0.10 \cdot F_{u,est}$ and $0.40 \cdot F_{u,est}$:

$$K_{SLS,1040} = \frac{0.40 \cdot F_{u,est} - 0.10 \cdot F_{u,est}}{v_{40} - v_{10}} \tag{2.13}$$

Where $F_{u,est}$ is the estimated load-carrying capacity of the joint (or the load at which failure is defined) and v_{10} and v_{40} correspond to the displacement at the load level of $0.10 \cdot F_{u,est}$ and $0.40 \cdot F_{u,est}$, respectively.

The yielding point signs the passage from elastic to plastic region. It is a fundamental point to define to calculate the ductility [13], [43]. The yielding point can be defined in different ways as summarized and discussed in [12], [14]. The resulting value of ductility can vary up to 60 % depending on which ductility definition is used [15]. In Karacabeyli and Cecotti [44], the yielding point is identified as the point corresponding to a load level equal to $0.5 \cdot F_u$, while in EN 2512 and SIA 265 [45], [46] it is defined as the intersection of the initial stiffness K_{SLS} and the tangent with inclination equals to $\frac{1}{6} \cdot K_{SLS}$ (Figure 2.14(a)). Also in Yasamura and Kawai [47], the yielding point is defined as the intersections of stiffnesses. In this the second stiffness is defined as a secant between 40% and 90% of load-carrying capacity F_u (Figure 2.14(b)). The point is then projected onto the load-displacement curve. Another common methodology is the equivalent energy elastic–plastic curve (EEEP) [48], illustrated in Figure 2.14(c). This method defines a linear-elastic graph whose underlying area is equivalent to that below the actual load-displacement curve. The linear region is defined up to the point corresponding to $0.40 \cdot F_u$. In [12], different methods to compute the yielding point are compared and it is found that the value of the yielding point based on the modified method of EN 12512 [45] is the most appropriate. Since EN 12512 [45] identifies a yielding point not belonging to the actual load-displacement curve, the modified version projects this point onto the curve.

With the identification of the yielding point, the ductility can be defined. Different definitions of ductility exist in standards and literature. An overview of the different definitions of ductility for joints can be found in [13], [43]. These

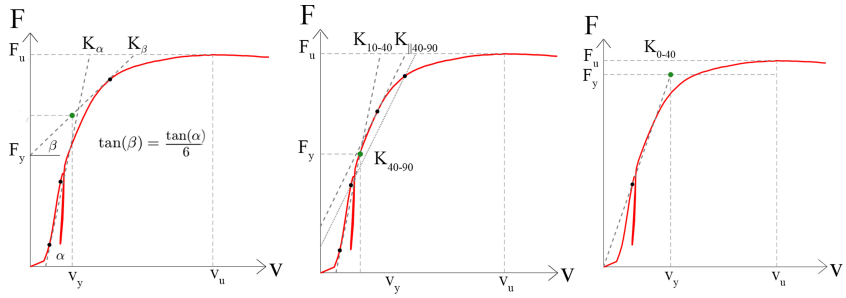

(a) EN 12512 and SIA 265 (b) Yamasura and Kawai (c) EEEP

Figure 2.14: Methods to determine the yielding point. Pictures taken from [15]

definitions are displacement or energy-based, relative or absolute. Displacement-based definitions are written not only in dependency of the displacement at yielding point v_y but also in dependency of the ultimate displacement v_u (displacement in correspondence of F_u) or displacement at failure v_f (after F_u has been reached). The most common displacement-based definition of relative ductility are:

$$D_{r,f} = \frac{v_f}{v_y} \tag{2.14}$$

$$D_{r,u} = \frac{v_u}{v_y} \tag{2.15}$$

The corresponding absolute definitions are:

$$D_{a,f} = v_f - v_y \tag{2.16}$$

$$D_{a,u} = v_u - v_y \tag{2.17}$$

The most common energy-based definition of ductility are:

$$E_u = \int_{v=0}^{v=v_u} f(F,v)dv \tag{2.18}$$

$$E_f = \int_{v=0}^{v=u_f} f(F,v)dv \tag{2.19}$$

Other definitions can be found in literature [12], [13], [29].

2.3.2 Analytical models

The definitions of K_{SLS} and F_u and ductility describe the load-displacement behaviour of joints as elastic-perfectly plastic. A more sophisticated way to approximate load-displacement curves of joints is through analytical models.

Analytical models are mathematical expressions that can describe the non-linearity of joints behaviour. These models consist in analytical expressions, i.e. exponential or logarithm functions, polynomials, rational functions [29], [49]–[52]. The models of Foschi and Richard-Abbott possess a physical interpretation of parameters. In the Foschi model (Equation 2.20), the parameters are the initial stiffness K_{in}, plastic stiffness K_p and the intercept of the plastic tangent with the vertical axis F_t:

$$F(v) = (F_t + K_p \cdot v)(1 - e^{(\frac{-K_{in} \cdot v}{F_t})}) \tag{2.20}$$

The Richard-Abbott model (Equation 2.21) adds an extra parameter a_1, which regulates the shape of the transition between the elastic and the plastic region. This parameter makes the curve "more flexible" compared to the Foschi model.

$$F(v) = \frac{(K_{in} - K_p) \cdot v}{(1 + (\frac{(K_{in} - K_p)}{F_t})^{a_1})^{\frac{1}{a_1}})}^{+} K_p \cdot v \tag{2.21}$$

Polynomials (Equation 2.22) are flexible and continuous functions. Even the most complex shapes can be approximated if a sufficiently high grade is selected.

$$F(v) = \sum_{n=1}^{k} p_i \cdot v^i \tag{2.22}$$

The Glos and the Brandner models are rational functions whose coefficients are determined by imposing certain boundary conditions [51], [52]. The rational functions are flexible, however they might be discontinuous in correspondence of the roots of the denominator. The model of Glos is dependent on five coefficients c_1, c_2, c_3, c_4, c_5 and it is expressed as:

$$F(v) = \frac{v + c_1 \cdot v^{c5}}{c_2 + c_3 \cdot v + c_4 \cdot v^{c5}} \tag{2.23}$$

The values of the coefficients c_1 to c_4 can be determined from the characteristics of the load-displacement curve through the application of the boundary conditions in Equation 2.24-2.27, while c_5 is a shape parameter. Two conditions are imposed on the derivative: the first imposes that the initial stiffness is equal to K_{in} (Equation 2.24), and the second says that the inclination of the curve in the point of the maximum load has to be equal to K_u. Usually, K_u is set to zero. The other two conditions are the passage of the curve through the point at maximum load F_u and asymptotic load level F_a that the curve has to approach for large displacements.

$$\frac{\mathrm{d}F}{\mathrm{d}x}(v = 0) = K_{in} \tag{2.24}$$

$$\frac{\mathrm{d}F}{\mathrm{d}x}(v = v_u) = K_u \tag{2.25}$$

$$F(v = v_u) = F_u \tag{2.26}$$

$$F(v >> v_u) = F_a \tag{2.27}$$

The Brander model [52] is a modification of the Glos model. It considers an initial shift v_{in} for the description of the initial consolidation region of the curve, a linear branch between v_{in} and v_{lin}, and the asymptotic load level for large displacement is set to zero. The resulting equation of the Brandner model is:

$$F = \frac{v}{c_1 + c_2 \cdot (v - v_{in}) + c_3 \cdot (v - v_{in})^{c_4}} \tag{2.28}$$

The modified equations for the calculating the coefficients c_1 to c_3 of Equation 2.28 are defined as follows:

$$c_1 = \frac{1}{K_{in}} \tag{2.29}$$

$$c_2 = \frac{1}{F_u - K_{in} \cdot (v_{lin} - v_{in})} - \frac{c_4}{K_{in} \cdot (v_u - v_{lin}) \cdot (c_4 - 1)} \tag{2.30}$$

$$c_3 = \frac{1}{(c_4 - 1) \cdot K_{in} \cdot (v_u - v_{lin})^{c_4}} \tag{2.31}$$

c_4 is the shape model parameter. Other models for the description of the load-displacement curves of joints can be found in literature, e.g. [29].

2.3.3 Design of timber joints according to standards

Stiffness

EC5 [7] refers to EN 26981 [16] for the determination of the stiffness at SLS for dowelled joints $K_{SLS,v}$ in the SLS and gives equations for different types of fasteners (Equation 2.32 and Equation 2.33). The proposed equation for pre-drilled fasteners, such as dowels, bolts, screws or nails is as follows:

$$K_{SLS,v} = \frac{\rho_m^{1.5} \cdot d}{23} \tag{2.32}$$

For nails without pre-drilling is as follows:

$$K_{SLS,v} = \frac{\rho_m^{1.5} \cdot d}{30} \tag{2.33}$$

$K_{SLS,v}$ is defined in dependency of the diameter of the fastener (d [mm]) and the mean value of the density (ρ_m [kg/mm^3]). The origin of the equations is explained in [53]: the stiffness is derived from the ratio between the load and the displacement v_{40}. The displacement at v_{40} is the displacement at

$0.4 \cdot F_u$ where F_u is determined according to the EYM. The relevant equations of the EYM are those for a nail in single shear in the failure mode with two plastic hinges per shear plane. The calculation is done without considering any safety factors. The displacement at 40% is taken from the studies [54], [55] on nailed joints. The equation contained in EC5 [7] were reported in the German standard DIN 1052 [56] based on characteristic density, while in EC5 the mean values of densities are used.

In the Swiss standard SIA 265 [46], the equation for the determination of K_{SLS} for dowels, bolts and pre-drilled nails is the following:

$$K_{SLS,v} = 3 \cdot \rho_k^{0.5} \cdot d^{1.7} \tag{2.34}$$

For nails without predrilling, all loaded parallel to the grain is the following:

$$K_{SLS,v} = 60 \cdot d^{1.7} \tag{2.35}$$

Equation 2.34 is in dependency of the diameter and the characteristic value of the density ρ_k [kg/mm^3] and Equation 2.35 only in function of the diameter. The loading direction in SIA 265 [46] are taken into account by reducing the values of $K_{SLS,v}$ by 50% when joints are loaded perpendicular to the grain.

Regarding joints with GiR, no equations for K_{SLS} for single rods loaded in tension exist in the current version of EC5 [7]. In the last draft version of EC5 from 2003 (in Annex C of EN 1995-2) [8], [57], equations for K_{SLS} are given for joints with GiR inserted parallel (Equation 2.36) and perpendicular (Equation 2.37) to the grain. They are both dependent on the mean value of the density of the timber and on the diameter of the rod. However, Annex C was disregarded in the published version of the standard [7].

$$K_{SLS,\parallel} = 0.04 \cdot d \cdot {\rho_m}^{1.5} \tag{2.36}$$

$$K_{SLS,\perp} = 0.08 \cdot d \cdot {\rho_m}^{1.5} \tag{2.37}$$

Regarding joints realised with laterally-loaded self-tapping screws (STS), K_{SLS} is determined with the same equations as used for laterally-loaded dowels and, consequently, by means of Equation 2.32. The current version of EC5 does not indicate how to determine the withdrawal stiffness of STS [7].

In the draft of the next generation of EC5 [10] Equations on how to calculate the axial stiffness of threaded rods, STS (Equation 2.38) and GiR (Equation 2.39) at SLS are included. The equation for axial stiffness $K_{SLS,ax}$ for threaded rods and STS is the following:

$$K_{SLS,ax} = 160 \cdot \frac{\rho_m}{420}^{0.85} \cdot d^{0.9} \cdot l_w^{0.6} \tag{2.38}$$

The equation for axial stiffness $K_{SLS,ax}$ for GiR is instead:

$$K_{SLS,ax} = 2 \cdot d^{0.6} \cdot l_w^{0.6} \cdot \rho_m^{0.9} \tag{2.39}$$

Where l_w[mm] is the withdrawal length. For laterally-loaded joints with GiR and STS in both current EC5 and SIA 265 the same rules for laterally-loaded dowels and bolts apply (Equations 2.32,2.33,2.35,2.34).

For joints with inclined STS, the draft of the next generation of EC5 of EC5 [10] specifies the K_{SLS} as a combination of lateral ($K_{SLS,v}$) and axial stiffness ($K_{SLS,ax}$), giving the following equation:

$$K_{SLS} = K_{SLS,v} \cdot \sin\epsilon \cdot (\sin\epsilon - \mu\cos\epsilon) + \frac{1}{2} \cdot K_{SLS,ax} \cdot \cos\epsilon \cdot (\cos\epsilon + \mu\sin\epsilon) \quad (2.40)$$

Where ϵ is the inclination of the fastener and μ is the friction coefficient.

Since the load-displacement behaviour of joints is non-linear, the tangential stiffness decreases with increasing displacement. To take into account the non-linear behaviour of joints at ULS, current EC5 [7] specifies that the stiffness at ULS K_u has to be taken as:

$$K_u = \frac{2}{3} \cdot K_{SLS} \quad (2.41)$$

No further indication of the interpretation of this equation is given in the standard. Therefore, it is not clear if K_u should be interpreted as the secant stiffness between the origin and the maximum load F_u or between the origin and the failure load F_f [15].

Load-carrying capacity

The load-carrying capacity of laterally-loaded dowelled joints can be calculated with the so-called European Yield model (EYM), based on the work of Johansen [58] and Meyer [59]. The different failure modes involve the embedment failure of the timber and/or the ductile failure of the dowels and are written in dependency of timber thickness. The relevant material properties are the embedment strength of the timber member and the yield moment of the fastener [15].

Regarding the load-carrying capacity of joints with GiR, a variety of different approaches are available in the literature, which is based on different definitions of the adhesive joints (strength analysis, linear fracture mechanics, non-linear fracture mechanics) [8], [9]. The draft of EC5 of 2003 [57] included a design approach in Annex C, that was developed from the results of the GIROD project and based on the generalized Volkersen theory. According to this approach, the characteristic axial load-carrying capacity of a single axially loaded rod in tension $R_{ax,k}$ should be taken as the minimum between the tensile capacity of the rod and the withdrawal capacity:

$$R_{ax,k} = min\left(f_{y,k} \cdot A_{ef}, \pi \cdot d_{equ} \cdot l_a \cdot f_{ax,k} \cdot \frac{tan\omega}{\omega}\right) \quad (2.42)$$

where $f_{y,k}$ [N/mm^2] is the yielding strength of the steel, A_{ef}[mm]^2 is the effective cross-sectional area of the rod, d_{equ}[mm] is the equivalent rod diameter, f_{ax} is taken equal to 5 [N/mm^2], l_a [mm] is the anchorage length,

$\omega = (0.016 \cdot l_a)/\sqrt{d_{equ}}$. This equation is appropriate when the failure of a joint is located in the adhesive and not at the interface between the timber and the adhesive or the adhesive and the rod [9], [60]. It is suitable for the pull-compression case and conservative in the case of pull-tension [9].

In the German design code DIN 1052 from 2004 [56], the design load-carrying capacity of axially loaded single rods parallel or perpendicular to the grain $R_{ax,d}$ is reported as the minimum between the design tensile capacity of the rod and the design value of the bondline capacity of the rod:

$$R_{ax,d} = min\left(f_{y,d} \cdot A_{ef}, \pi \cdot d \cdot l_{ad} \cdot f_{k1,d}\right) \tag{2.43}$$

Where $f_{y,d}$ [N/mm^2] is the design yielding strength of the rod, l_{ad}[mm] is the glued length, and $f_{k1,d}$ [N/mm^2] is the design value of the bondline strength, that depends on the glued length.

The draft of the next generation of EC5 [10] gives the following equation to calculate the load-carrying capacity of axially loaded single rods, as the minimum between the tensile capacity of the steel rod and the withdrawal capacity of the rod along the bondline:

$$R_{ax,Rd} = min\left(R_{t,d}, R_{w,d}\right) \tag{2.44}$$

Where the withdrawal capacity $R_{w,d}$ is determined from the minimum between the characteristic bondline shear capacity and failure strain of the timber:

$$R_{w,k} = min\left(\pi \cdot l_{ad,ef} \cdot f_{w,k}, E_s \cdot A_s \cdot \epsilon_{u,timber}\right) \tag{2.45}$$

$\pi \cdot l_{ad,ef} \cdot f_{w,k}$ represents the characteristic bondline shear capacity, where $l_{ad,eff}$[mm] is the effective withdrawal length (equivalent to previously defined l_{ad}), $f_{w,k}$ [N/mm^2] is the characteristic withdrawal (bondline) strength. ϵ_u is the failure strain of the timber parallel to the grain, and A_s is the nominal stress area.

For joints axially and laterally-loaded at the same time, the following equation in EC5 can be used from the interaction [7]:

$$\left(\frac{F_{ax,Ed}}{R_{ax,Rd}}\right)^2 + \left(\frac{F_{v,Ed}}{R_{v,Rd}}\right)^2 \leq 1 \tag{2.46}$$

Where $R_{ax,Rd}$ is the design resistance of the fastener in tension. For screw loaded in tension, $R_{ax,Rd}$ is taken as the minimum between the tensile resistance of the screw, the withdrawal capacity of the threaded part of the screw. If the screw is loaded in compression, the buckling resistance of the screw should be considered as well. Equation 2.46 addresses generally joints with combined lateral and axial loading of the fastener, but not specifically shear joints with inclined fastener. In [61], the equation was compared against experiments on shear joints with inclined fasteners and it was found that the equation is not able to satisfactorily predict the increase in load-bearing capacity when the angle between the fastener and the load increases, while it is unsafe for STS

under shear-compression. Another approach proposed in [62] provides a better estimation of the load-carrying capacity of joints with inclined STS:

$$R = R_v \cdot (\cos\{\epsilon\} - \mu \cdot \sin\{\epsilon\}) + R_{ax} \cdot (\sin\{\epsilon\} + \mu \cos\{\epsilon\}) \tag{2.47}$$

The load-carrying capacity is expressed as a function of lateral capacity R_v and axial capacity R_{ax} of the joint with inclined STS, where μ is the friction coefficient and ϵ is the load-to-screw axis angle. In EC5 [7], the load-carrying capacity of a single axially loaded screw is taken as the minimum of the withdrawal failure of the threaded part of the screw, the tear-off failure of the screw head of screws used in combination with steel plates, the pull-through resistance of the screw head, the buckling failure of the screw if loaded in compression.

The withdrawal resistance of screws is calculated in function of the effective length of the screw l_{ef} [mm], diameter d [mm] and characteristic withdrawal strength perpendicular to the grain f_{ax} [N/mm^2] and α the angle between the fastener and the load direction:

$$R_{ax,k} = \frac{f_{ax,k} \cdot d \cdot l_{ef} \cdot k_d}{1.2 \cdot \cos^2 \alpha + \sin^2 \alpha} \tag{2.48}$$

Equation 2.48 is used if the diameter and inner diameter respect certain limitations. Otherwise, the withdrawal parameter $f_{ax,k}$ must be determined through experiments. To Equation 2.48 the reference density ρ_a must be added. The equation then becomes:

$$R_{ax,k} = \frac{f_{ax,k} \cdot d \cdot l_{el} \cdot k_d}{1.2 \cdot \cos^2 \alpha + \sin^2 \alpha} \cdot (\frac{\rho_k}{\rho_a})^{0.8} \tag{2.49}$$

Where the withdrawal parameter $f_{ax,k}$ must be determined through experiments. R_v is the resistance of the laterally-loaded screw, which is determined by applying the EYM. In the draft of the next generation of EC5 [10], some more advanced equations for the withdrawal strength are included. The axial tensile resistance $F_{ax,t,d}$ of axially loaded STS, is the minimum of the axial tensile resistance of each timber member $F_{ax,t,d,1}$ and the design axial tensile resistance of the fastener $F_{ax,t,d,2}$. $F_{ax,t,d,1}$ is calculated as the maximum between the pull-through capacity and the withdrawal capacity as the following:

$$F_{ax,t,d,1} = \frac{\max(F_{pull,k}, F_{w,k})}{\gamma_m} \tag{2.50}$$

Where the withdrawal capacity of the screw is calculated as follows:

$$F_{w,k} = \pi \cdot d \cdot l_w \cdot f_{w,k} \tag{2.51}$$

l_w [mm] is the anchorage length, $f_{w,k}$ [N/mm^2] is the characteristic withdrawal strength. Equation 2.51 is valid for nails, screws, and rods with wood screw thread. The equation for $f_{w,k}$ depends on the type of fastener and the diameter characteristics. For example, for screws characterized by 3.5 mm $\leq d \leq$ 22 mm and $0.55d \leq d_1 \leq 0.76d$, that $f_{w,k}$ for solid timber, CLT,

LVL, plywood is computed according to Equations 2.52 if $l_w \geq 5d$, $\rho_k \leq 700$ [kg/mm^3] and $d \geq 8$ mm.

$$f_{w,k} = k_{screw} \cdot k_w \cdot k_{mat} \cdot d^{-0.33} (\frac{\rho_k}{350})^{k_\rho} \tag{2.52}$$

Where k_{mat} is the material parameter for the number of laminations, k_w is the withdrawal parameter, k_ρ is the parameter related to the density. k_w is a parameter written in dependency of the inclination of the fastener and to the timber species. For Equation 2.52 it is taken as:

$$k_w = \begin{cases} 1.10 \text{ for softwoods and } 15° \leq \epsilon \leq 90° \\ 1.25 - 0.05\text{d for softwoods and } 0° \leq \epsilon \leq 15° \\ 1.6 \text{ for hardwoods and } 0° \leq \epsilon \leq 90° \end{cases} \tag{2.53}$$

If $l_w \geq 2.5\ d$ and $\rho \geq 350$ [kg/mm^3], $f_{w,k}$ is taken as 4 [N/mm^2]. The characteristic pull through capacity equation depends on the timber product and on geometrical parameters limit. For example, in the case of solid timber, plywood and CLT and if the thickness of the inner timber member is $> 4 \cdot d$, the Equation is the following:

$$F_{pull,k} = 14 \cdot {d_{head}}^{-0.4} \cdot (\frac{\rho_k}{350})^{0.8} \tag{2.54}$$

Where d_{head} [mm] is the head diameter of the fastener.

Ductility

While it is mentioned in EC5 there exists the possibility to re-distribute loads within the structure through joints of adequate ductility, no further explanation or ductility requirements are given for joints [15].

In EC8 (EN 1998) [63] , the standard for the seismic design of structures, ductility classes for timber structures are provided. It is specified that in order to classify timber structures as medium ductility capacity and high ductility capacity, the "dissipative zone" has to possess a static ductility ratio of at least 4 and 5, respectively.

Also in the draft of the next generation of EC5 more specific indications about ductility levels are lacking. However, indications on how to achieve ductile failure in the case of joints with axially loaded rods are provided. In fact, it is specified that to archive ductility of joints with axially loaded GiR, the yield failure of the rods should occur prior to the brittle modes of timber or the brittle failure of the bondline. This requirement is achieved by checking that the following condition is satisfied:

$$F_{t,0.95} < F_{w,k} \tag{2.55}$$

Where $F_{t,0.95}$ is the 95th-percentile of the resistance of the rod, defined as follows:

$$F_{t,0.95} = A_s \cdot f_{y,0.95} \tag{2.56}$$

Where $A_s[mm^2]$ is the nominal stress area for threaded rods or nominal cross-sectional area for ribbed rod and $f_{y,0.95}$ is the 95th percentile of the resistance of the rod. According to the draft of the next generation of EC5 [10], laterally-loaded dowelled joints can be considered ductile if the joint develops two plastic hinges per shear plane.

In Standard SIA 265 [46] two different levels of ductility based on Equation 2.14 are defined. A ductility ratio D_f between 1 and 2 represents joints that fail in a brittle way without major displacement capacity, i.e. dowelled and bolted joints that develop less than two hinges per shear plane. A ductility ratio $D_f \geq 2$ corresponds to dowelled and bolted joints that develop two plastic hinges per shear plane.

Smiths et al. in [64] give an approach to classify fasteners in timber structures based on ductility ratios (see Table 2.5). The classification gives the possibility to group certain joints based on their load-displacement behaviour. The ductility values are calculated following the Equations 2.14 and 2.16 and they are based on the indications provided in EC8 [63].

Table 2.5: Classification of relative and absolute ductility according Smiths et all [64]

Classification	Smiths et al. [64]	
	[-]	[mm]
Brittle	$D_{r,f} \leq 2$	$D_{a,f} \leq 1$
Low Ductility	$2 < D_{r,f} \leq 4$	$1 < D_{a,f} \leq 3$
Moderate Ductility	$4 < D_{r,f} \leq 6$	$3 < D_{a,f} \leq 6$
High ductility	$D_{r,f} > 6$	$D_{a,f} > 6$

2.3.4 Load-displacement shapes of timber joints

Analytical expressions to determine the stiffness, the load-carrying capacity of dowelled joints, joints with GiR and joints with STS use as input the main geometrical, mechanical and loading influential parameters. However, joints behaviour in general is affected by many more factors, not included in the analytical expressions.

An overview of most influential parameters in given in Figure 2.15 and more details on how these parameters affect the load-displacement curve can be found in Paper II.

Due to the large number of influencing parameters of joints behaviour and to the variety of joints configurations in timber, the shapes of the load-displacement curves of timber joints show great diversity. For joints with dowels and bolts, typical shapes are represented in Figure 2.16. The curves can present all the three regions previously identified: the zero-stiffness region, the elastic region and the plastic one. The joint can show brittle behaviour, with the curve only showing in elastic behaviour (curve D1 in Figure 2.16). The plastic region can be characterized by a plastic plateau (curve D2 in Figure 2.16) or it can show a hardening branch, with no clear identification of the load-carrying

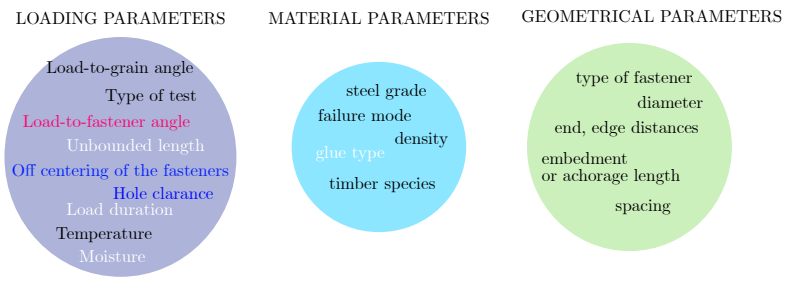

Figure 2.15: Main parameters of influence

capacity. The plastic region can be also characterized by a softening branch, such as curve D4 in Figure 2.16. The curve can also show extensive plastic displacement with a hardening behaviour (curves D4 and D5 in Figure 2.16).

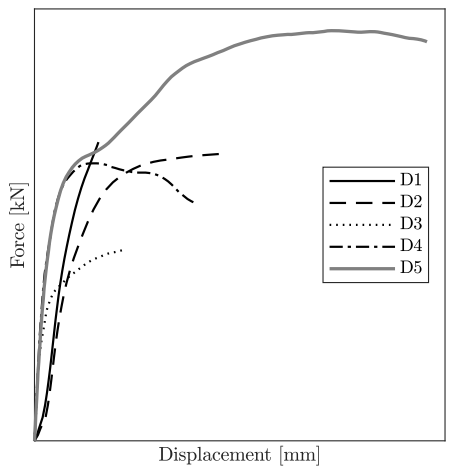

Figure 2.16: Typical load-displacement curves of joints with dowel [65], [66]

For joints with GiR where the bondline fails, the load-displacement curve can show a rather brittle behaviour (G1 in Figure 2.17) or a load-displacement curve with peak and softening behaviour (G2 in Figure 2.17). If properly designed and yielding of the rod is achieved, the joints with GiR can also show hardening and ductile behaviour (curve G3 in Figure 2.17). Laterally-loaded GiR show a soft and plastic behaviour, similar to joints with laterally-loaded dowels (curve G4 in Figure 2.17).

The behaviour of joints with STS is largely influenced by the load-to-screw axis angle. If the angle is equal to 90°, the joints show a very soft but ductile behaviour, with a pronounced hardening branch (curve S1 in Figure 2.18).

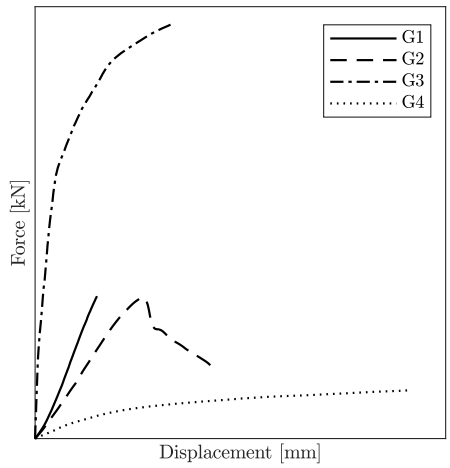

Figure 2.17: Typical load-displacement curves of joints with dowel [65], [66]

When the angle is set to less than 90°, then the load-displacement curve shows a more stiff but less ductile behaviour (S2, S3 and S4 in Figure 2.18).

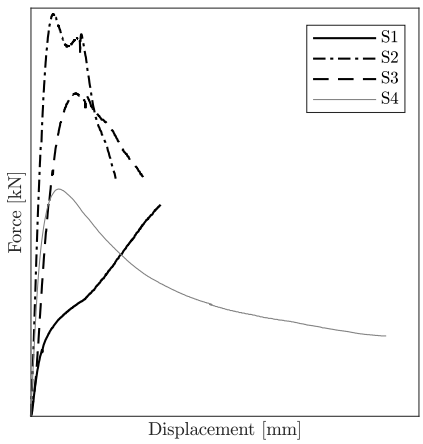

Figure 2.18: Typical load-displacement curves of joints with dowel [65], [66]

Chapter 3

Reliability estimation of the structure

In this chapter the probability failure domain of the case study of a beam with rotational springs at the supports is described in terms of possible failure modes. A comparison among methods to estimate the reliability of the structure on the case study is conducted in terms of computational time and accuracy.

3.1 Case study

A typical example of a statically indeterminate structure is a beam with rotational springs at the supports at its ends. This simple system can be considered as representative of one element of a portal frame structure or of a dome structure with semi-rigid joints. Once the timber member is "extracted" from the global structure, the influence of the joints behaviour on the reliability of such structure can be studied. In this simple system, the effect of joint stiffness on the elastic distribution of the load can be illustrated in Figure 3.1.

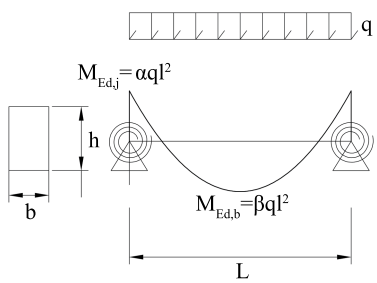

Figure 3.1: Beam with semi-rigid joints

Where α and β are two coefficients written in function of the elastic stiffness

of joints K_{el} and the bending stiffness EI of the beam:

$$\alpha = \frac{K_{el}L}{24EI + 12K_{el}L} \tag{3.1}$$

and

$$\beta = \frac{1}{8} - \alpha. \tag{3.2}$$

3.2 Implementation

The failure domain in the case of the statically indeterminate structure of a beam restrained by semi-rigid joints (Figure 3.1) can be described by multiple limit state equations. In Paper I the following three failure modes were distinguished:

1. The bending resistance of the beam or the bending resistance of the joint is reached, while the joints remain fully elastic and before the plastic region of the joints is entered (Brittle failure mode);

2. The bending resistance of the beam or the bending resistance of the joint is reached, after entering into the plastic region of the joints (Ductile failure mode 1);

3. The ultimate rotational capacity of the joints is reached before the bending resistance of the beam or the bending resistance of joint is reached (Ductile failure mode 2);

Further details about the description and implementation of the three failure modes in the limit state equations can be found in Paper I.

3.3 Methodology

The input variables considered for the analysis are represented in Table 3.1. For the input variables marked with "*", the probabilistic distributions suggested Joint Committee on Structural Safety (JCSS) were adopted [37]. The characteristic load $q = 4.6\frac{kN}{m}$ was chosen based on the design according to EC5 for the beam with GIR joint. The calculations are based on timber C24 as material. The probabilistic analysis was conducted with UQLab toolbox [67]. The maximum sample size was set as stopping criteria for MCS, Subset, IS. MCS was tested setting the maximum sample size equals to 10^7 and 10^6. The initial value m_0 for the Active learning algorithm was set to 10. The algorithm was stopped when the maximum samples size was reached or the default convergence criteria was met.The final results of failure probability are illustrated in Figure 3.2 in dependency of D_u.

The resulting probabilities of failure are summarized in Table 3.2 in the case of $D_u = 20$. MCS (maximum sample size equals to 10^6) returned good estimation of the probability of failure in relatively low computational time. The accuracy can be improved by increasing the sample size but at expenses

Table 3.1: Distribution parameters of the considered random variables

Input	Unit	Distribution	Mean V.	Char. V.	CoV
$q*$	$\frac{kN}{m}$	Gumbel	-	4.6	0.4
f_m*	$\frac{N}{mm^2}$	Lognormal	37	24	0.25
K_{el}	$\frac{kNm}{rad}$	Lognormal	1000	-	0.3
D_u	-	Lognormal	1 to 20	-	0.1
$M_{R,j}$	kNm	Lognormal	18.4	-	0.2
$E*$	$\frac{N}{mm^2}$	Lognormal	11,000	-	0.13
W_{el}	m^3	Constant	0.001	-	
L	m	Constant	6.5	-	-

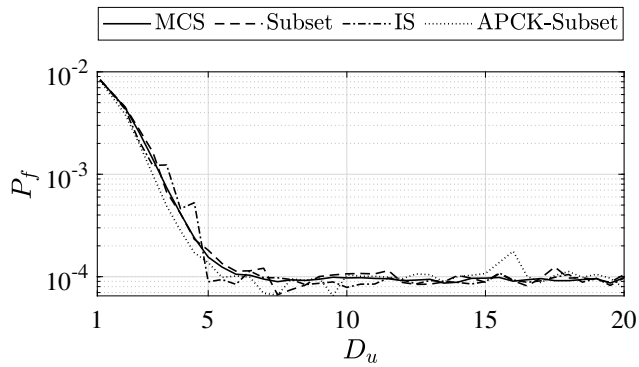

Figure 3.2: Comparison of the convergence of different modelling techniques

of the computational time. For example, increasing the sample size from 10^6 to 10^7 resulted in increased computational time by a factor of ≈ 45.

Subset and IS needed a lower number of samples but less than MCS, however with less accuracy if compared to MCS with sample size of 10^{-7}. The results on this example partially confirmed the results on the illustration example illustrated in Subsection 2.2.3. However, in this case, APCK-Subset showed quite poor convergence for the majority of cases and it did not return a satisfactory estimation of the probability of failure. This is probably due to the fact that the number of input variables and limit state equations are higher. The failure domain is more difficult to approximate for APCK-Subset.

Table 3.2: Results for $D_u = 20$.

Method	Evaluations	P_f	CV	Time
MCS	10^7	$2.85e^{-4}$	0.02	89.44 sec
MCS	10^6	$2.76e^{-4}$	0.06	2.18 sec
Subset	36998	$2.56e^{-4}$	0.09	0.17 sec
IS	1196	$2.94e^{-4}$	0.07	0.32 sec
APCK-Subset	162	$4.02e^{-4}$	0.02	1211 sec

Chapter 4

Results and discussion

In this chapter the results of the parametric study on beam with semi-rigid joints are presented. The suitability of analytical models presented previously is tested on a selection of load-displacement curves from the literature.

4.1 Parametric study

In a parametric study the mean value of the ductility D_u for the three types of joints (DTF joint, GiR joint and finger joint) was varied. The chosen methodology was MCS, setting the maximum number of samples equal to 10^6.

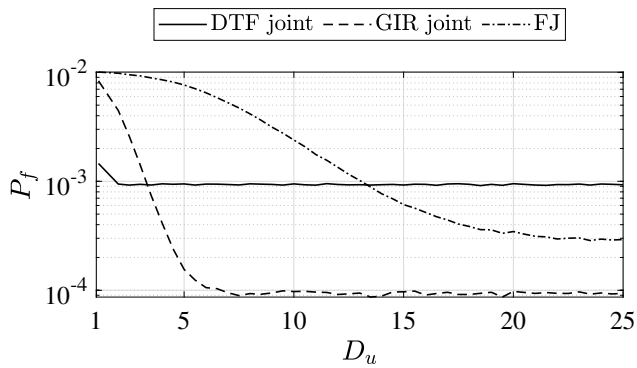

Figure 4.1: Variation of the probability of failure with different values of ductility.

Results showed that the ductility had no impact on the joints with lower stiffness, while it had much more impact on joints characterized by medium or high stiffness. This is expected since the beam is designed for higher stiffness than the stiffness of the DTF joint, so the failure occurs at mid-span and not at joint for these cases. Therefore, in this case the ductility cannot be utilized. For the other two types of joints, the load can be redistributed if the bending capacity of the joints is exceeded. However, after a certain threshold,

the ductility has no longer an impact on the probability of failure of the beam. For example, for GIR joints with a value of D_u exceeding 6, the probability of failure has no longer impact on the probability of failure of the system. For FJ joints, the range of ductility values with a change in probability of failure is larger. However, the probability of failure changes to a lesser extent than in the case of GIR joint for increasing ductility. A sensitivity study was performed by computing the Pearson coefficient for each type of joint and for each value of mean ductility. The relative plots are shown in Paper I. The sensitivity study underlined how the variability of stiffness affects the reliability of structures if the failure is located at midspan of the beam (DTF joint), while the uncertainties coming from ductility are relevant when the failure is located at the joints (GiR and FJ joints) It should be noted that in practice a large absolute value of ductility may be much harder to be achieved for relatively stiff joint systems such as FJ or GIR joints.

4.2 Load-displacement curves of joints

The analysis on a simple but representative statically indeterminate structures showed that the stiffness is an important prerequisite to design reliable structures and that is the system is properly design, the ductility of joints can be used to optimize the structural system. The mechanical behaviour of timber joints can be really diverse and highly non-linear. This should be reflected by design rules, which are often simplistic and do not reflect the variety and the actual load-displacement behaviour of joints. For example, at ULS the elastic stiffness is simply reduced by a constant factor to take into account the non-linear behaviour (Equation 2.41).

In Figure 4.2 the ratio $\frac{K_{sec}}{K_{sec,1040}}$ is represented against the ratio of the load level at which the secant stiffness is computed and the load-carrying capacity of the joint F_u. $K_{sec,10,40}$ is the secant stiffness according to Equation 2.13, while F_u is taken as the maximum force or the force at displacement of 15 mm, whatever occurred first.

The ratio $\frac{K_{sec}}{K_{1040}}$ decreases to $\frac{2}{3}$ when a load level of $80\% - 100\% \cdot F_u$ is reached. This is not true for curves that present brittle behaviour (curve D1) for which this ratio always remains close to 1. Assuming that the joint will attract more load than in reality at ULS, can be an unsafe assumption in the case of a statically indeterminate structure, leading to an increased probability of failure [14].

The ductility of selected timber joints is examined in Figure 4.3. The relative D_r and absolute ratio D_u of load-displacement curves of selected timber joints is examined. The ductility classification presented in [64] is used and the yielding point is identified according to the modified version of EN 12512 [45] methodology proposed in [12]. v_f is chosen as the point that corresponds to the failure, the point in correspondence of a load drop of $0.2 \cdot F_u$ or at a maximum displacement of 30 mm, whatever occurred first (as indicated in [45]).

As it can be observed in Figures 4.2 and 4.3, the current design rules are not always suitable to represent the actual mechanical behaviour of joints

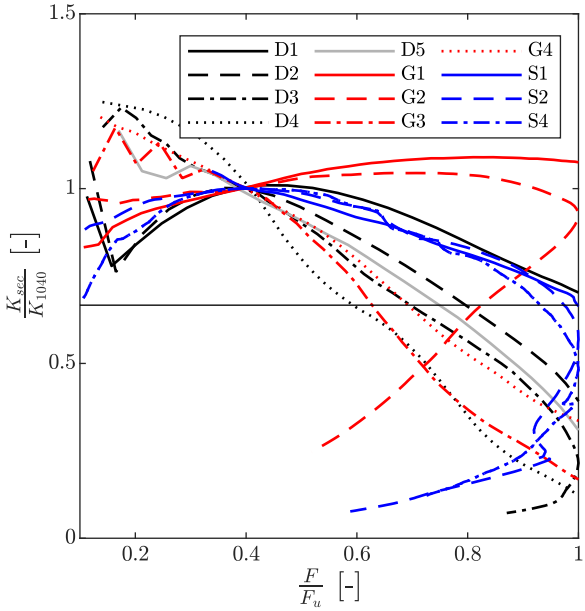

Figure 4.2: Relation of secant stiffness K_{sec} to secant stiffness K_{1040} along different load levels of the representative load-displacement curves

in a satisfactory way. Currently, the entire ductile mechanical behaviour is disregarded and assuming a smaller stiffness at ULS might be unsafe in case of brittle failure mode of joints. Moreover, the different equations for K_{SLS} in design standards do not take into account the variability of stiffness.

In the light of outcomes of the parametric and sensitivity study of the structure and the analysis of load-displacement curves of timber joints, the need for a precise description of timber joints is underlined. Analytical models can provide a good approximation of non-linear behaviour of timber joints, however information on the suitability of these model in the ability to approximate the diverse types of load-displacement curves are missing. In the following chapter, different analytical models are presented and their suitability to model diverse and complex joint behaviour is evaluated.

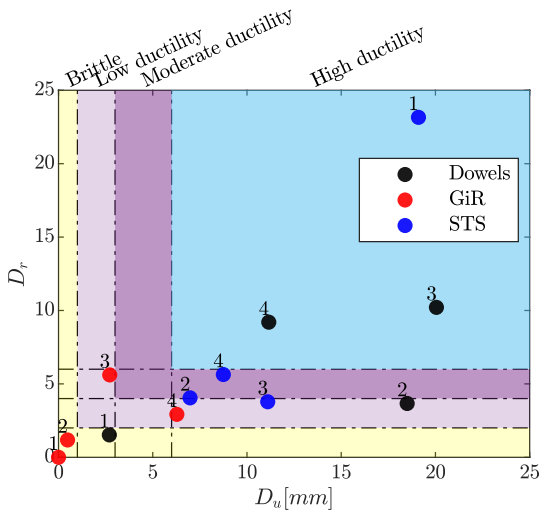

Figure 4.3: Interaction of the relative D_r and absolute D_a. The values for curve D5 is excluded from the representation since it exceeds the representation intervals (D_r,$D_a > 25$)

4.2.1 Model fit

Three curves from the selected load-displacement curves of joints are shown in Figure 4.5 to underline the main differences among the regression models. The experimental curves show different behaviour in the plastic region: the curve represented in Figure 4.5(a) is characterized by simultaneous presence of two plastic plateau, the curve in Figure 4.5(b) is characterized by strong hardening effect and the curve in 4.5(c) shows a complex softening branch.

The absolute error of the regression in the first (elastic) region of the curves is shown in Figures 4.5(d), 4.5(e), 4.5(f) while the goodness of the fit for all the examined load-displacement curves is represented in Figure 4.4 in terms of R-squared R^2. R-squared is the ratio of the sum of squares regression (SSR) and the sum of squares total (SST). The sum of Squares Regression (SSR) represents the total variation of all the predicted values found on the regression line or plane from the mean value of all the values of response variables. The sum of squares total (SST) represents the total variation of actual values from the mean value of all the values of response variables (see Equation 4.1).

$$R^2 = 1 - \frac{SSR}{SST} = 1 - \frac{\sum y_i - \tilde{y}}{y_i - \bar{y}} \tag{4.1}$$

The goodness of the fit for the load-displacement curves is measured in terms of R^2 as reported in Figure 4.4.

The Foschi model overestimates the initial region of the curve, in particular when the curve possesses a softening behaviour. The Richard-Abbott model overestimates the initial stiffness less than the model of Foschi. Both the Foschi and Richard-Abbott models can approximate the softening branch only linearly. Some characteristics of the load-displacement curves, such as a highly non-linear softening branch cannot be approximated by the Foschi or and Richard-Abbott model. If a sufficiently elevated grade is selected, the polynomial model can approximate every possible shape. If the grade is not sufficiently elevated, the polynomial can show wavy shapes if fitted on complex shapes.

The coefficients of the Glos and the Brandner models are determined by imposing the specified boundary conditions. These models have been developed to approximate curves that shows a softening branch. For the curve of the Type S1, the local maximum has been replaced by the yielding point. However, the models are still not able to approximate the hardening branch of curve S1 (Figure 4.5(b)). Among all the curves, the model of Richard-Abbott, even if it only possesses four coefficients, is able to provide a satisfactory approximation of all the analyzed curves (Figure 4.4).

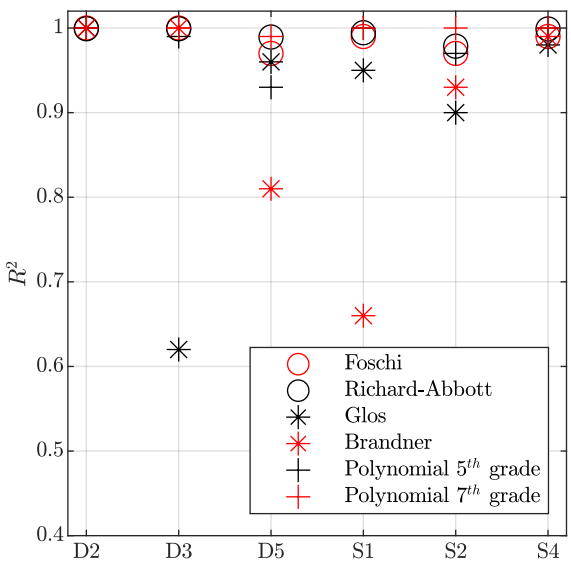

Figure 4.4: R^2 coefficient for all the curves and regression models

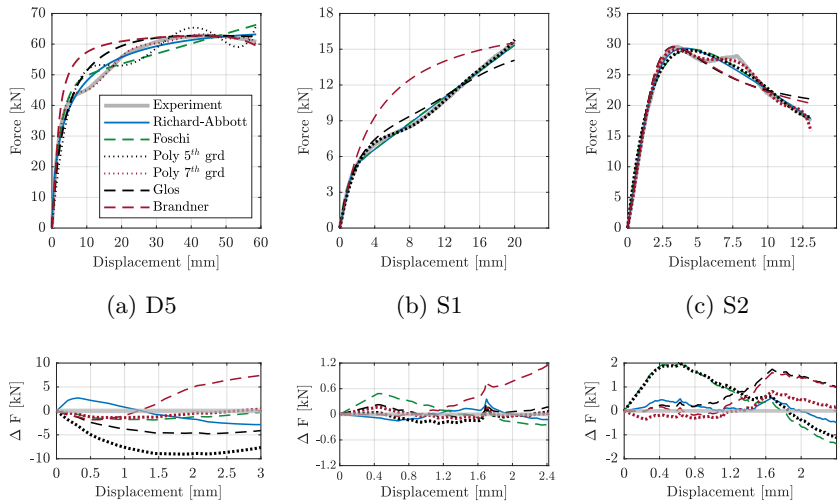

(a) D5 (b) S1 (c) S2

(d) D5 Residuum (e) S1 Residuum (f) S2 Residuum

Figure 4.5: Application of parameterization equations to different types of experimentally determined slip curves.

4.2.2 Stability of the model

The variability in the load-displacement behaviour of timber joints arises amongst others from the natural variability of the material used but also the variability in geometry and assembly. Therefore, one important characteristic of a suitable regression model is its ability to represent the variability of the load-displacement behaviour. The polynomial model instead, if enough elevated grade is selected, is able to approximate even more complex curve shape. For that reason, the two models are selected and the stability of both of them was tested on available experimental data from [68] and the results presented in this chapter.

The selected experimental data are timber-to-timber joints with inclined STS, i.e. the series S1-S3 with different numbers of specimens per series. The model is considered to be stable if a relatively small change in the data results in a small change in the estimated value of the parameters of the model. The coefficients of the Richard-Abbott model and the polynomial model are reported in Table 4.1 and 4.2.

The actual distribution type of the parameters is unknown since only a few repetitions for each specimen are available. Therefore, normal distributions for each parameter have been assumed. The curve in correspondence of each set of parameters was plotted in correspondence of each set of sampled parameters.

$$F(v) = a_i \cdot v^7 + b_i \cdot v^6 + c.v^5 + e \cdot v^5 f \cdot v^4 + g \cdot v^3 + h \cdot v^2 + h \cdot v \qquad (4.2)$$

Where $a_i, b_i, c_i, d_i, e_1, f_i, g_i$ are the i-th realization of the parameters.

Table 4.1: Coefficients of the Richard-Abbott model for the dataset on STS

Angle [°]	n_{test}	K_{in} $[\frac{kN}{mm}]$ (CoV)	K_p $[\frac{kN}{mm}]$ (CoV)	F_t $[kN]$ (CoV)	a_1 $[-]$ (CoV)
High density					
90	3	3.84	0.52	4.31	5.51
60	4	7.31 (7%)	-0.70 (21%)	31.06 (12%)	2.57 (20%)
45	7	16.22 (10%)	-2.38 (32%)	49.88 (19%)	2.55 (38%)
Low density					
90	3	2.48	0.35	3.73	3.36
60	4	5.23 (10%)	-0.61 (18%)	24.73 (11%)	2.24 (15%)
45	8	12.04 (13%)	-1.64 (29%)	33.69 (17%)	2.11 (30%)

Table 4.2: Coefficients of 7^{th} grade polynomial model for the data set on joints with self-tapping screws

Angle [°]	a $\frac{kN}{mm^7}$	b $\frac{kN}{mm^6}$	c $\frac{kN}{mm^5}$	d $\frac{kN}{mm^4}$	e $\frac{kN}{mm^3}$	f $\frac{kN}{mm^2}$	g $\frac{kN}{mm^1}$
High density							
90	3.29e-7	-2.74e-5	9.73e-4	-2.04e-2	0.20	-1.29	4.57
60	-2.09e-6 (44%)	1.52e-4 (39%)	-4.36e-3 (34%)	0.06 (29%)	-0.39 (26%)	0.38 (59%)	7 (5%)
45	-1.46e-4 (60%)	6.61e-3 (52%)	-0.12 (46%)	1.01 (40%)	-4.21 (37%)	5.36 (54%)	12.96 (15%)
Low density							
90	6.77e-7	-4.73e-5	1.36e-4	-0.021	0.19	-1.01	3.30
60	-2.28e-6 (35%)	1.61e-4 (31%)	-4.46e-3 (27%)	0.061 (25%)	-0.39 (26%)	0.66 (61%)	4.55 (19%)
45	-2.17e-5 (703%)	1.57e-3 (347%)	-3.57e-2 (215%)	0.35 (154%)	-1.50 (135%)	0.83 (463%)	11.00 (34%)

$$F(v) = \frac{(K_{i,in} - K_{i,p}) \cdot v}{(1 + (\frac{(K_{i,in} - K_{i,p})}{F_{i,t}})^{a_{i,1}})^{\frac{1}{a_{i,1}}})^{+} K_{p,i} \cdot v \tag{4.3}$$

Where $K_{i,in}, K_{i,p}, F_{i,t}, a_{i,1}$ are the i-th realization of the Richard-Abbott model parameters. The stability was tested on the curve with the load-to-screw axis angle equal to 60° in the case of high density. The parameters were sampled independently, but their correlation was considered. The statistical dependency between variables is accounted through Pearson's correlation coefficient. Given a pair of random variables (X, Y), the equation for the Pearson coefficient is:

$$\rho = \frac{cov(x, y)}{\sigma_x \cdot \sigma_y} \tag{4.4}$$

For the parameters determined according to the Richard-Abbott model, the correlation matrix is given in Table 4.3 .

Based on the results in Figures 4.6(a) and 4.6(b), it can be observed that the realizations of the polynomial are far from being close to the experimental curves. In contrast, the realizations of the Richard-Abbott model are close to experimental curves. Therefore, the variability of polynomial coefficients (CoVs) is not related to the variability of the input data but rather related to fitted noise. The instability of the polynomial model and the large scatter of coefficients makes the value of coefficients unreliable. This means that polynomial models,

Table 4.3: Correlation matrix of Richard-Abbott parameters

	K_{in}	K_p	F_t	α
K_{in}	1	0.4758	0.33	0.65
K_p	0.488	1	0.91	0.93
F_t	0.33	0.92	1	0.72
α	0.65	0.93	0.739	1

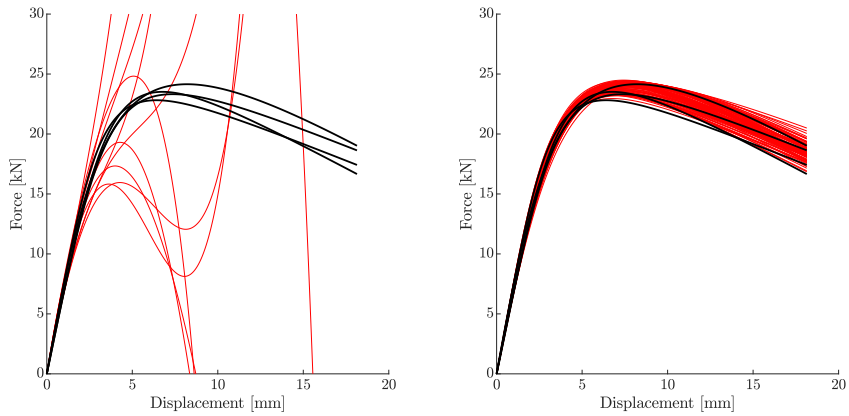

(a) Stability of the polynomial model (b) Stability of the Richard-Abbott model

Figure 4.6: Stability of the models. In black are experimental curves, in red the realizations of the models

although able to approximate very complex load-displacement curves, cannot be used to represent the variability of experimental data.

On the contrary, the Richard-Abbott model is stable since a variation in input data results in a small variation in the estimated parameters of the model. The Monte-Carlo study with generated curves from the probabilistic distribution of model parameters further demonstrated the ability of the Richard-Abbott model to represent the variability of experimental data.

Chapter 5

Conclusions and future work

5.1 Conclusions

A parametric study assuming an elastic-perfectly plastic behaviour for the joints has been performed on a simple but representative statically indeterminate structure. The uncertainties from the applied loads, the resistance of the beam, and the load-displacement characteristics of the joints have been considered.

From the probabilistic analysis, the following conclusions can be drawn:

- The elastic stiffness and ductility are the two main joint characteristics impacting the reliability of the structure. Ductility is particularly important for the case of GIR joints and FJ.
- Current deterministic considerations of stiffness and ductility of joints are inadequate for proper analysis of statically indeterminate structures. Instead, the reliability estimation of a structure allows to consider the system effects that otherwise would not be considered. This enables the full optimization of the safety of the structure.
- Methods like MCS can be difficult to apply when a large number of samples are required to compute the probability of failure of the structural system, in particular when computationally heavy models are used. Other methods such as IS, Subset, or metamodel-based methods, can be used to overcome this issue.

In the structural analysis, elastic-perfectly plastic behaviour of joints has been assumed. However, elastic-perfectly plastic behaviour is not representative of actual joints in timber structures in practice. Therefore, a more precise description of the non-linear load-displacement behaviour of joints is needed. The Foschi, Richard-Abbott, polynomial, Glos, and Brandner models have been fitted to relevant shapes of load-displacement curves from the literature. The following conclusions can be drawn:

- The Foschi and Richard-Abbott models are suitable to represent load-displacement curves both with and without softening. However, the softening can just be approximated linearly;
- The Glos model and the polynomials, if a sufficiently elevated grade is selected, offer the possibility to approximate the initial slip. In all the other models the initial slip can be considered by adding an initial shift to the curves;
- The Polynomial model is useful to approximate very complex shapes of load-displacement curves. However, they are not stable and they cannot describe the variability of test data;
- The Richard-Abbott model is the most appropriate one among the examined models. This is underlined by the high value of R-squared obtained for all the examined curves and by the ability to represent the variability of test data.

5.2 Future work

An overview of future work is illustrated in Figure 5.1. The work in this thesis has been mainly based on the level of the entire structure. In addition, the first input for the development of the level of the single-fastener joint has been covered. A suitable analytical model has been selected for the ability to represent complex non-linear load-displacement curves and the associated variability. The following objectives are suggested for future research at the single-fastener level:

- To conduct experiments on single-fasteners joints, varying most influential parameters of the load-displacement behaviour;
- To parametrize experimental load-displacement curves through analytical model;
- To quantify the probabilistic distributions of the model parameters.

The following is suggested for the multi-fasteners joint level:

- To develop the model for multi-fastener joint (component method, finite element models), by the use of the model of single-fastener joint as input;
- To validate the model.

The structural analysis by means of MCS will be updated with a more realistic description of the multi-fastener joint and its associated variability.

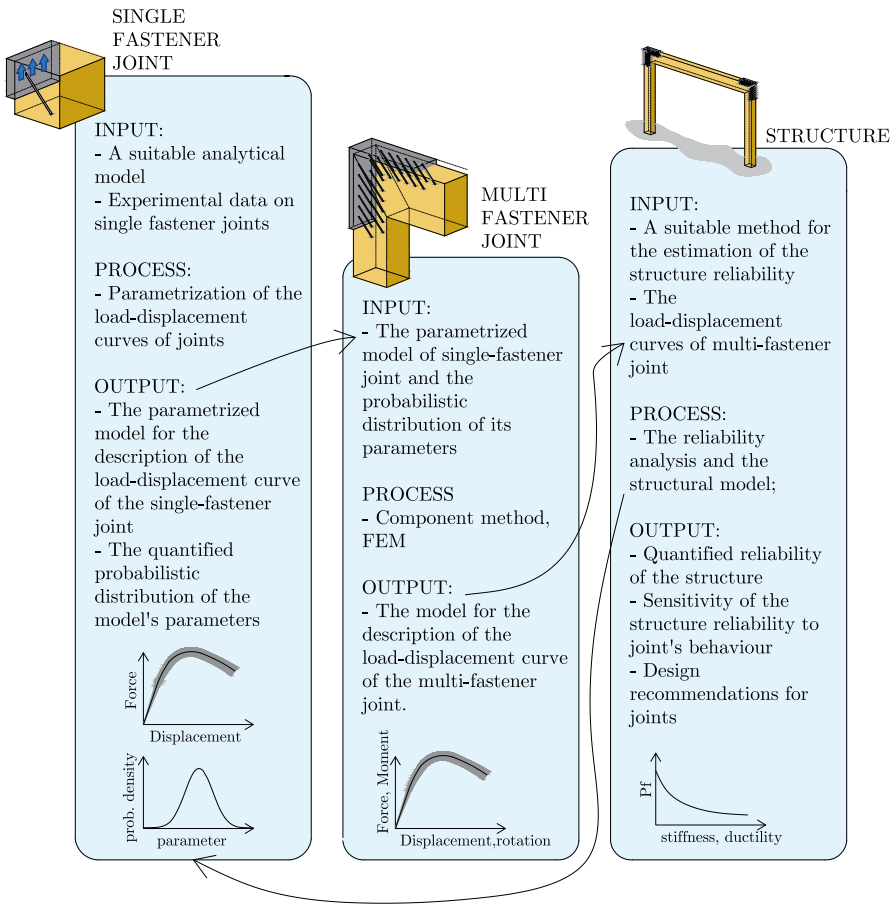

Figure 5.1: Overview of the presented and future work

Copyright attribution

- Figure 1.1(a): Creative Commons Horyu-ji National Treasure World heritage https://en.wikipedia.org/wiki/H%C5%8Dry%C5%AB-ji#/media/File:Horyu-ji_National_Treasure_World_heritage_%E5%9B%BD%E5%AE%9D%E3%83%BB%E4%B8%96%E7%95%8C%E9%81%BA%E7%94%A3%E6%B3%95%E9%9A%86%E5%AF%BA85.JPG by Nekosuki CC BY 4.0 https://creativecommons.org/licenses/by-sa/4.0/ cropped from the original
- Figure 1.1(b): Creative Commons St Andrew's Church from the south-west https://en.wikipedia.org/wiki/Greensted_Church#/media/File:'Church_of_St_Andrew'_Greensted,_Ongar,_Essex_England_-_from_the_south-west.JPG
  by Acabashi https://commons.wikimedia.org/wiki/User:Acabashi
  CC BY 4.0
  https://creativecommons.org/licenses/by-sa/4.0/ cropped from the original
- Figure 2.5(a) Messe Frankfurt Hall © Max Bögl/WIEHAG Timber Construction, reprinted with permission by WIEHAG Timber Construction
- Figure 2.5(b) Messe Frankfurt Hall © Messe Frankfurt GmbH/Arch. Hascher Jehle/WIEHAG Timber Construction, reprinted with permission by WIEHAG Timber Construction
- Figure 2.8(a) © Ermanno Acler/Holzpak Engineering Srl
- Figure 2.8(b) © Ermanno Acler/Holzpak Engineering Srl
- Figure 2.9(a) © Oliver Jaist Fotografie
- Figure 2.9(b) © Oliver Jaist Fotografie
- Figure 2.10(a) Canary Whalf © Foster + Partner/WIEHAG Timber Construction, reprinted with permission by WIEHAG Timber Construction
- Figure 2.10(b) Crossrail detail © Foster and Partners/Nigel Young/WIEHAG Timber Construction, reprinted with permission by WIEHAG Timber Construction

Bibliography

[1] W. Pryce, *Buildings in Wood: The History and Traditions of Architecture's Oldest Building Material*. Rizzoli, 2005.

[2] S. Kulturhus, *Building in wood has a distinguished past and a bright future*. [Online]. Available: https://www.mynewsdesk.com/se/sarakulturhus/news/building-in-wood-has-a-distinguished-past-and-a-bright-future-433140.

[3] M. Schweigler, T. K. Bader, G. Hochreiner and R. Lemaître, "Parameterization equations for the nonlinear connection slip applied to the anisotropic embedment behavior of wood," *Composites Part B: Engineering*, vol. 142, pp. 142–158, 2018, ISSN: 1359-8368. DOI: 10.1016/j.compositesb.2018.01.003.

[4] J. Köhler, *Reliability of timber structures*. 2007, 212 S. DOI: 10.3929/ETHZ-A-005454370.

[5] *NZS AS 1720.1:2022 Timber structures Part 1: Design methods*. Standards Association of Australia, Standards New Zealand, 2022.

[6] L.-M. Ottenhaus, R. Jockwer, D. van Drimmelen and K. Crews, "Designing timber connections for ductility – a review and discussion," *Construction and Building Materials*, vol. 304, p. 124 621, 2021, ISSN: 0950-0618. DOI: 10.1016/j.conbuildmat.2021.124621.

[7] *EN 1995-1-1: Eurocode 5: Design of Timber Structures - Part 1-1: General - Common Rules and Rules for Buildings*. Bruxelles, Belgium: European Committee for Standardization CEN, 2004.

[8] M. Stepinac, F. Hunger, R. Tomasi, E. Serrano, V. Rajcic and J.-W. Van de Kuilen, *Comparison of design rules for glued-in rods and design rule proposal for implementation in European standards*. Aug. 2013.

[9] G. Tlustochowicz, E. Serrano and R. Steiger, "State-of-the-art review on timber connections with glued-in steel rods," *Materials and Structures/Materiaux et Constructions*, vol. 44, pp. 997–1020, Jun. 2011. DOI: 10.1617/s11527-010-9682-9.

[10] *prEN 1995-1-1: Eurocode 5 Design of timber structures — Part 1-1: General rules and rules for buildings. CEN/TC 250/SC 5 N 1650*. Bruxelles, Belgium: European Committee for Standardization CEN, Dec. 2022.

[11] J. J. Mack, *The strength and stiffness of nailed joints under short-duration loading* (Division of Forest Products technological paper). Melbourne, Australia: Commonwealth Scientific and Industrial Research Organization, Australia, 1966.

[12] F. Brühl, "Ductility in timber structures - possibilities and requirements with regard to dowel type fasteners," PhD Thesis, Universität Stuttgart, Munich, Germany, 2020.

[13] A. Jorissen and M. Fragiacomo, "General notes on ductility in timber structures," *Engineering Structures*, vol. 33, no. 11, pp. 2987–2997, 2011. DOI: 10.1016/j.engstruct.2011.07.024.

[14] D. Caprio, R. Jockwer and M. al-Emrani, "Reliability of statically indeterminate timber structures: Modelling approaches and sensitivity study," in *Current Perspectives and New Directions in Mechanics, Modelling and Design of Structural Systems*, CRC Press, 2022, pp. 1649–1655, ISBN: 9781003348443. DOI: 10.1201/9781003348443-270.

[15] R. Jockwer, D. Caprio and A. Jorissen, "Evaluation of parameters influencing the load-deformation behaviour of connections with laterally loaded dowel-type fasteners," *Wood Material Science & Engineering*, vol. 17, pp. 1–14, Jul. 2021. DOI: 10.1080/17480272.2021.1955297.

[16] *EN 26891 - Timber structures - Joints made with mechanical fasteners - General principles for the determination of strength and deformation characteristics*. Bruxelles, Belgium: European Committee for Standardization CEN, 1991.

[17] R. Crocetti, "Large-span timber structures," in *Proceedings of the World Congress on Civil, Structural, and Environmental Engineering*, 2016, pp. 1–23. DOI: 10.11159/icsenm16.124.

[18] K.-H. Gotz, D. Hoor, K. Mohler and J. Natterer, *Timber Design and Construction Sourcebook: a comprehensive guide to methods and practise*. McGraw-Hill publisher company, 1989.

[19] H. Stamatopoulos, K. A. Malo and A. Vilguts, "Moment-resisting beam-to-column timber connections with inclined threaded rods: Structural concept and analysis by use of the component method," *Construction and Building Materials*, vol. 322, p. 126 481, 2022. DOI: https://doi.org/10.1016/j.conbuildmat.2022.126481.

[20] A. Leijten, "Requirements for moment connections in statically indeterminate timber structures," *Engineering Structures*, vol. 33, pp. 3027–3032, 2011. DOI: 10.1016/j.engstruct.2011.03.014.

[21] A. S. Rebouças, Z. Mehdipour, J. M. Branco and P. B. Lourenço, "Ductile moment-resisting timber connections: A review," *Buildings*, vol. 12, no. 22, p. 240, Feb. 2022, ISSN: 2075-5309. DOI: 10.3390/buildings12020240.

[22] S. Schilling, "Structural behaviour and reliability of timber trusses with dowelled steel-to-timber connections," PhD Thesis, ETH Zurich, Zurich, Switzerland, 2022. DOI: 10.3929/ethz-b-000538109.

[23] A. Brunauer, "Messehalle 11 frankfurt, frankfurt trade fair hall," in *Proc. of the 15. Internationales Holzbau-Forum IHF*, Garmisch-Partenkirchen, Germany, 2009.

[24] E. Acler, "Nanyang technological university sports hall, singapore," in *Proc. of the 23. Internationales Holzbau-Forum IHF*, Garmisch - Partenkirchen, Germany, 2017.

[25] A. Manuello, "Semi-rigid connection in timber structure: Stiffness reduction and instability interaction," *International Journal of Structural Stability and Dynamics*, vol. 20, p. 2 050 072, Jun. 2020. DOI: 10.1142/S0219455420500728.

[26] J. Chilton and G. Tang, *Timber gridshells: architecture, structure and craft*. Taylor & Francis, 2016.

[27] K. A. Malo, R. B. Abrahamsen and M. A. Bjertnæs, "Some structural design issues of the 14-storey timber framed building "treet" in norway," *European Journal of Wood and Wood Products*, vol. 74, no. 3, pp. 407–424, May 2016, ISSN: 1436-736X. DOI: 10.1007/s00107-016-1022-5.

[28] T. Green and J. Taggart, *Tall Wood Buildings : Design, Construction and Performance*. Basel/Berlin/Boston: Walter de Gruyter GmbH, 2017.

[29] G. Flatscher, *Evaluation and approximation of timber connection properties for displacement-based analysis of CLT wall systems* (Monographic Series TU Graz: Timber Engineering & Technology), English, G. Schickhofer and R. Brandner, Eds. Verlag der Technischen Universität Graz, 2017, vol. TET 6, ISBN: 978-3-85125-557-7.

[30] G. D'Arenzo, D. Casagrande, A. Polastri, M. Fossetti, M. Fragiacomo and W. Seim, "Clt shear walls anchored with shear-tension angle brackets: Experimental tests and finite-element modeling," *Journal of Structural Engineering*, vol. 147, no. 7, p. 04 021 089, Jul. 2021.

[31] F. Brühl, U. Kuhlmann and A. Jorissen, "Consideration of plasticity within the design of timber structures due to connection ductility," *Engineering Structures*, vol. 33, pp. 3007–3017, 2011. DOI: 10.1016/j.engstruct.2011.08.013.

[32] J. Köhler and M. Baravalle, "Risk-based decision making and the calibration of structural design codes – prospects and challenges," vol. 36, pp. 55–72, Jan. 2019, ISSN: 1028-6608. DOI: 10.1080/10286608.2019.1615477.

[33] W. M. Bulleit, "Uncertainty in structural engineering," *Practice Periodical on Structural Design and Construction*, vol. 13, no. 1, pp. 24–30, Feb. 2008, ISSN: 1084-0680. DOI: 10.1061/(ASCE)1084-0680(2008)13:1(24).

[34] *ISO2394 - General principles on reliability for structures*. International Organisation for Standardisation, 2015.

[35] JCSS, *Risk Assessment in Engineering - Principles, System Representation & Risk Criteria*. Joint Committee on Structural Safety, www.jcss-lc.org, 2008.

[36] M. Baravalle and J. Köhler, "A risk-based approach for calibration of design codes," *Structural Safety*, vol. 78, pp. 63–75, Jan. 2019. DOI: 10.1016/j.strusafe.2018.12.003.

[37] JCSS, *Probabilistic Model Code*. Joint Committee on Structural Safety, www.jcss-lc.org, 2006.

[38] F. G. J. Köhler R. Steiger and R. Jockwer, *Assessment of selected eurocode based design equations in regard to structural reliability*, Växjö, Sweden, Aug. 2012.

[39] W. Fauriat and N. Gayton, "Ak-sys: An adaptation of the ak-mcs method for system reliability," *Reliability Engineering and System Safety*, vol. 123, pp. 137–144, 2014.

[40] S.-K. Au and J. Beck, "Estimation of small failure probabilities in high dimensions by subset simulation," *Probabilistic Engineering Mechanics*, vol. 16, pp. 263–277, 2001. DOI: 10.1016/S0266-8920(01)00019-4.

[41] M. Moustapha, S. Marelli and B. Sudret, *A generalized framework for active learning reliability: Survey and benchmark*, 2021. arXiv: 2106.01713 [stat.CO].

[42] J. M. B. Bichon and S. Mahadevan, "Efficient surrogate models for reliability analysis of systems with multiple failure modes," *Reliability Engineering and System Safety*, vol. 96, pp. 1386–1395, 2011. DOI: 10.1016/j.ress.2011.05.008.

[43] K. A. Malo, J. Siem and P. Ellingsbø, "Quantifying ductility in timber structures," en, Modelling the Performance of Timber Structures, vol. 33, pp. 2998–3006, Nov. 2011, ISSN: 0141-0296. DOI: 10.1016/j.engstruct.2011.03.002.

[44] E. Karacabeyli and A. Ceccotti, "Quasi-static reversed-cyclic testing of nailed joints," in *Proc. of the CIB-W18 Meeting 29/29-7-7*, Bordeaux, France, 1996.

[45] *EN12512 - Timber structures - Test methods - Cyclic testing of joints made with mechanical fasteners.* Bruxelles, Belgium: European Committee for Standardization CEN, 2002.

[46] *SIA 265 - Timber structures.* Swiss Society of Engineers and Architects, 2012.

[47] M. Yasumura, "Estimating seismic performance of wood-framed structures," in *Proceedings of 5th WCTE*, vol. 2, Montreux, Switzerland, 1998, pp. 564–571.

[48] G. C. Foliente, in *Issues in seismic performance testing and evaluation of timber structural systems. In: Proc. of the International Wood Engineering Conference, October 28–31*, 1996.

[49] R. O. Foschi, "Load-slip characteristics of nails," *Wood science*, vol. 7, pp. 69–76, 1974.

[50] R. M. Richard and B. J. Abbott, "Versatile elastic-plastic stress-strain formula," EN, *Journal of the Engineering Mechanics Division*, vol. 101, no. 4, pp. 511–515, Aug. 1975. DOI: 10.1061/JMCEA3.0002047.

[51] P. Glos, "Zur bestimmung des festigkeitsverhaltens von brettschichtholz bei druckbeanspruchung aus werkstoff-und einwirkungskenngrößen," PhD Thesis, Berichte zur Zuverlässigkeitstheorie der Bauwerke, No. 35/78, Technische Universität München, Munich, Germany, 1978.

[52] R. Brandner, A. Ringhofer and M. Grabner, "Probabilistic models for the withdrawal behavior of single self-tapping screws in the narrow face of cross laminated timber (CLT)," en, *European Journal of Wood and Wood Products*, vol. 76, no. 1, pp. 13–30, 2018, ISSN: 1436-736X. DOI: 10.1007/s00107-017-1226-3.

[53] J. Ehlbeck and H. Larsen, "Eurocode 5 - design of timber structures: Joints," *International Workshop on Wood Connectors*, pp. 9–23, 1993, ISSN: 0935018565.

[54] J. Ehlbeck and H. Werner, "Design of joints with laterally loaded dowels. proposals for improving the design rules in the cib code and the draft eurocode 5," en, in *Proceedings of 21 Meeting of the CIB-W18 Meeting 21/21-7-4*, Parksville, Canada, 1988a.

[55] J. Ehlbeck and H. Werner, "Untersuchungen über die tragfähigkeit von stabdübelverbindungen," *Holz als Roh- und Werkstoff*, vol. 46, no. 8, pp. 281–288, Aug. 1988b, ISSN: 1436-736X. DOI: 10.1007/BF02615055.

[56] *DIN 1052: Entwurf, Berechnung und Bemessung von Holzbauwerken - Allgemeine Bemessungsregeln und Bemessungsregeln für den Hochbau.* Berlin, Germany: DIN Deutsche Institut für Normung e.V, 2008.

[57] *CEN (2003) Minutes of the sixteenth meeting of Document CEN/TC 250/SC 5: N 209.* European Committee for Standardization CEN, Oct. 2003.

[58] K. W. Johansen, "Theory of timber connections," 1949.

[59] A. Meyer, "Die tragfähigkeit von nagelverbindungen bei statischer belastung," de, *Holz als Roh- und Werkstoff*, vol. 15, no. 2, pp. 96–109, Feb. 1957, ISSN: 1436-736X. DOI: 10.1007/BF02609174.

[60] R. Widmann, R. Steiger and E. Gehri, "Pull-out strength of axially loaded steel rods bonded in glulam perpendicular to the grain," en, *Materials and Structures*, vol. 40, no. 8, pp. 827–838, 2007, ISSN: 1871-6873. DOI: 10.1617/s11527-006-9214-9.

[61] R. Tomasi, A. Crosatti and M. Piazza, "Theoretical and experimental analysis of timber-to-timber joints connected with inclined screws," *Construction and Building Materials*, vol. 24, pp. 1560–1571, 2010. DOI: 10.1016/j.conbuildmat.2010.03.007.

[62] I. Bejtka and H. Blaß, *Joints with inclined screws*, 2002.

[63] *EN 1998-1:2004: Eurocode 8: Design of structures for earthquake resistance - Part 1: General rules, seismic actions and rules for buildings.* European Committee for Standardization CEN, 2004.

[64] I. Smith, A. Asiz, M. Snow and I. Chui, "Possible canadian/iso approach to deriving design values from test data," in *Proc. of the Meeting 39 of Working Commission W18 - Timber Structures, CIB-W18, Paper No. 39-17-1*, Florence, Italy, 2006.

[65] A. Jorissen, "Double shear timber connections with dowel type fasteners," *Heron*, vol. 44, Jan. 1999.

[66] J. Gauß and U. Kuhlmann, "Consideration of the connection stiffness in design process - experimental investigation," en, in *Proc. of the World Conference on Timber Engineering WCTE2018*, Seoul, Korea, 2018, p. 7.

[67] *UQLab: A Framework for Uncertainty Quantification in MATLAB*, 2014, pp. 2554–2563.

[68] R. Jockwer, R. Steiger and A. Frangi, "Fully threaded self-tapping screws subjected to combined axial and lateral loading with different load to grain angles," in *Materials and Joints in Timber Structures*, S. Aicher, H.-W. Reinhardt and H. Garrecht, Eds., Dordrecht: Springer Netherlands, 2014, pp. 265–272, ISBN: 978-94-007-7811-5.